SURFACE MODIFICATION OF ELECTROSPUN POLY(VINYLIDENE FLUORIDE) NANOFIBROUS MICROFILTRATION MEMBRANE

SATINDERPAL KAUR
(B.Sc (Hons), NUS)

A THESIS SUBMITTED

FOR THE DEGREE OF MASTER OF ENGINEERING

NANOSCIENCE & NANOTECHNOLOGY INITIATIVE (NUSNNI)

NATIONAL UNIVERSITY OF SINGAPORE

Acknowledgements

I would like to take this opportunity to thank my supervisor, Prof. Seeram Ramakrishna, for believing in me and supporting me to pursue my masters. He has constantly supervised and encouraged me throughout my research. I would also like to express my most sincere gratitude to Emeritus Prof. Matsuura for introducing the research of membrane science to me and has truly inspired me.

I am deeply indebted to Dr. Ma Zuwei, Dr. Kotaki Masaya and Renuga Gopal for their guidance, support and advice in the experimental work. I would also like to take this opportunity to thank Renuga Gopal for being a dear, close and wonderful friend. I am also thankful to Dr. Subramanian Sundarrajan for his comments and suggestions. I would also like to express my appreciation to Dr. Thomas Yong for his help, invaluable advice from time to time and being a friend. He has made the laboratory a very fun and lively place to work in. To my colleagues Teo Chieh Yin Karen, Teo Wee Eong, Wang Yanping Karen, Ramakrishnan Ramaseshan, Kazutoshi Fujihara and Ryuji Inai, whom I have truly enjoyed working with. To Evelyn Ng and Steffen Ng for handling all administrative work related to this thesis.

Without my family's constant love, support and encouragement, it would have been very difficult to complete this research. Last but not least I would like to thank WAHEGURU for blessing me always.

Table of Contents

Summary

Electrospinning has gained an increasing appeal in recent years and is capable of creating sub-micron to nanoscale fibers through an electrically charged jet of polymer solution/melt. These electrospun fibers have been explored in various applications such as scaffolds for tissue engineering, drug delivery carrier, biosensor/chemosensor, reinforced nanocomposite, electronic and semi-conductive materials. However their use in liquid separation is still at infancy. The main focus of the thesis would be to develop a high flux asymmetric microfiltration electrospun nanofibrous membrane (ENM) through surface modification. Another aspect of the thesis would explore the potential of ENM in separating microparticles. It is anticipated that the modified ENM would have smaller surface pores as compared to a non-modified ENM. Hence this surface modified ENM would be capable in separating smaller sized particles.

Poly(vinylidene fluoride) (PVDF) has been electrospun to generate fibers in the nanometer range. A solution of poly(vinylidene fluoride) (PVDF) in N,N-dimethylacetamide (DMAC) and acetone was electrospun to produce fibers in the nanometer range. This membrane was then subjected to a particle challenge test to better understand the separation capability of an as-spun ENM and was correlated with the bubble point obtained using a capillary flow porometer. The as-spun ENM was successful in rejecting more than 90% of 1, 5 and 10 μm particles. The ENM was able to retain its flux after separating 5 and 10 μm particles indicating that fouling did not take place. However for the 1 μm particle irreversible fouling took place and a

cake layer was formed which attributed to the high rejection rate of this particle size and a resultant low flux. Hence the as-spun ENMs were able to separate particles above 5 μm without any damage done to the membrane and these separation results were in line with the bubble point of the membrane which was identified as 3.2 μm from the porometer. Thus the porometer gives a good gauge in the separation ability of the ENM.

The surface of the electrospun nanofiber membranes (ENMs) was successfully modified with poly(methacrylic acid) (PMAA) to achieve bubble point and pore size distribution in the range of microfiltration membranes and sustained a high flux throughput. The surface of ENM and hydrophobic commercial PVDF membrane (HVHP) was exposed to argon plasma for different periods and was subsequently graft copolymerized with methacrylic acid (MAA). The grafting density was quantitatively measured with toluidine blue-O (TBO). The degree of grafting increased steeply with an increase of plasma exposure time for the ENM. However, the increase in the grafting density on the surface of commercial hydrophobic PVDF membranes (HVHP) was not as drastic and reached a plateau after some time. Field Emission Scanning Electron Microscopy (FESEM) micrographs revealed an alteration in the pore structure for both grafted membranes. The Liquid Entry Permeation of water (LEPw) dropped extensively for both membranes. Through surface modification, the grafted ENM bubble point was reduced to 0.88 μm and its pore size distribution was close to HVLP. In addition to this, water flux permeation studies revealed that the surface modified ENM had a better flux throughput than the commercial membranes attributed to its highly interconnected porous network. In

conclusion, by modifying the surface of the ENM the surface pores can be reduced while maintaining a porous base structure and hence being able to separate particles of different sizes at a high flux throughput.

List of Tables

List of Figures

Abbreviations and Symbols

Short form	Full name
AC	Acetone
Beaded ENM (A)	PVDF ENM with beads and fiber diameter is 249 ± 0.08 nm
Beaded ENM (B)	PVDF ENM with beads and fiber diameter is 472 ± 0.259 nm
DMAC	N,N-Dimethylacetamide
DMF	N,N-Dimethylformamide
DSC	Differential Scanning Calorimeter
ENM	Electrospun nanofibrous membrane
HVHP	Commercially available hydrophobic phase inverted PVDF
HVLP	Commercially available hydrophilic surface modified phase inverted PVDF
LEPw	Liquid Entry Pressure of water
MF	Microfiltration
NF	Nanofiltration
nm	Nanometer
NMP	1-Methyl-2-pyrrolidinone
PP	Polypropylene
ppm	Parts per million
PTFE	Polytetrafluroethylene
PVDF	Poly(vinylidene fluoride)

RO	Reverse Osmosis
S.D.	Standard Deviation
UF	Ultrafiltration
µm	Microns

List of Publications

Journals:

S. Kaur, M. Zuwei, R. Gopal, S. Ramakrishna, T. Matsuura
Plasma induced graft co-polymerization of poly(methacrylic acid) on electrospun poly(vinylidene fluoride) nanofiber membrane
Langmuir (In-press)

R. Gopal, **S. Kaur**, C. Feng, C. Chan, S.Ramakrishna, S. Tabe and T. Matsuura
Electrospun nanofibrous polysulfone membranes as pre-filters: particulate removal
J. Memb. Sci., 289, (2007) 210-219

R. Gopal, **S. Kaur**, Z.W. Ma, S. Ramakrishna and T. Matsuura
Electrospun Nanofibrous Filtration Membrane
J. Memb. Sci., 281 (2006) 581-586

S. Kaur, M. Kotaki, Z.W. Ma, R. Gopal and S. Ramakrishna.
Oligosaccharide Functionalized Nanofibrous Membrane
Int. J. of Nanosci., 5 (2006), 1-11

Conferences:

C. Feng, K.C. Khulbe, T. Matsuura, R. Gopal, **S. Kaur**, S. Ramakrishna,
*Preparation and Characterization of PVDF Electro-spun Nanofiber Membranes***,**
The North American Membrane Society, May 12-17, 2006, Chicago, Illinois, USA

S. Kaur, M. Kotaki, Z.W. Ma, R. Gopal and S. Ramakrishna
Oligosaccaharide Functionalized Nanofibrous Membrane
1st Nano-Engineering & Nano-Science Congress 2004, July 7-9, 2004, Singapore

Book Chapter:

R. Gopal, Z.W. Ma, **S. Kaur** and S. Ramakrishna
Surface Modification and Application of Functionalized Polymer Nanofibers (Chapter 4) *in "Molecular Building Blocks for Nanotechnology: From Diamondoids to Nanoscale Materials and Applications",* Edited by G.A. Mansoori, T.F. George, G.P. Zhang and L Assoufid, Springer-Verlag Series, USA, 2006

Chapter 1

Introduction

1.1 Polymer nanofibers

When the diameter of polymer fibers is reduced from micrometers to sub-microns or nanometers, they exhibit a large surface area to volume ratio which can be as large as 10^3 times of that of a microfiber [Huang (2003)]. These properties make them potential candidates for several applications such as molecular filtration, tissue engineering scaffolds, wound dressing, drug delivery, cosmetics, protective clothing against toxic and biological hazards, sensor devices and many more. The hypothesis is that, this unique parameter (large surface area to volume ratio) would improve performance in many applications manifold times [Seeram (2005)].

1.2 Nanofiber fabrication techniques

Polymeric nanofibers can be produced by a number of techniques such as drawing [Ondarcuhu (1998)], template synthesis [Feng (2002)], phase separation [Ma (1999)], self assembly [Liu (1996)] and electrospinning [Formhals (1934)]. Among all the methods, electrospinning is the only method that can be further developed for mass production and its simplicity and inexpensiveness has added a greater appeal to its usage. In addition to this, a wide variety of polymers can be transformed to nanofibers using this technique [Seeram (2005)].

1.3 Electrospun nanofibrous membrane (ENM)

Electrospinning is a straightforward and cost effective method to produce fibers from sub-micron to nanometer range. It is based on a simple principle whereby a polymer solution or melt that is held at the tip of an orifice by surface tension is subjected to a critical voltage. When the electrical force at the surface of the polymer solution or melt overcomes the surface tension, a charged jet is erupted. A grounded collector placed at a distance away will induce a potential difference to that of the charged solution at the tip of the spinneret. It is this potential difference that will cause the charged solution to accelerate towards the collector. With time, a fibrous mat can be collected.

1.4 Advantages of ENM

The electrospun nanofibrous web possesses attractive properties such as high porosities, interconnected open pore structure, pore sizes ranging from sub-micron to several micrometers, high permeability for gases, super hydrophobicity [Ma (2005), Miwa (2000)] and a large surface area per unit volume. Through electrospinning a variety of morphologies can be obtained such as porous fibers, hollow fibers, beaded fibers and many more which can be used for specific applications [Seeram (2005)]. In addition to this, the thickness of the overall membrane can be controlled. Some of these attributes make them highly attractive in separation technology. However the use of electrospun nanofiber membranes (ENMs) in liquid separation is limited and still in its infancy [Gopal (2006), Wang (2005), Yoon (2006), Zuwei (2006 a), Zuwei (2006 b)]. The open porous structure of the ENM will be the key parameter that will

influence the separation characteristics of particles. It is anticipated that a highly efficient fibrous membrane for liquid separation can be produced through electrospinning.

1.5 Stumbling block

However, the ENMs generated through electrospinning have a typical symmetrical structure. With symmetric membranes some degree of in-depth separation could occur as particles move through the tortuous flow path [Keith (1995)]. In addition to this, ENMs have interconnected pore size in the large micron scale and hence it is anticipated that the as-spun ENMs can only separate larger microparticles. As such they are only suitable as 'loose' microfiltration (MF) membranes, with a symmetrical structure.

1.6 Motivation

To broaden its use in separation technology, the surface pores of the ENMs should be further reduced. This can be achieved through surface modification and an asymmetric structure can be produced with proper optimization. An asymmetric membrane will have surface pores much less than those in the bulk of the membrane. These entrap the particles almost exclusively at the surface whilst still offering low hydrodynamic resistance [Keith (1995)].

1.7 Objective of study

The objective of the study is to:

"To develop a high flux asymmetric microfiltration electrospun nanofibrous membrane through surface modification"

This will be achieved based on the following approach:

- Optimizing the conditions of electrospinning to achieve fibers in the nanoscale and yet sustaining a high productivity rate.
- Optimization of surface modification conditions to develop a 'tighter' microfiltration ENM.
- Characterization of the surface modified ENMs to evaluate its membrane properties and performances and comparison will be made with a non-modified ENM.
- Comparison of water flux performance of the ENMs and commercial membranes.

1.8 Significance

Electrospinning will introduce a novel method of developing a high flux membrane where the surface properties can be tailored to separate particles of certain size range. This work opens up the avenue of exploring the use of nanofibers for more main stream application in the separation technology.

Chapter 2

Literature Review

2.1 Background of electrospinning

Electrospinning is far from a new technique that goes all the way back to 1902 [William (1902), Cooley (1902)]. It is only recently that this technique has received renewed attention because of its simplicity, versatility, low cost and scale controllability [Huang (2003)]. There are basically three components required to implement the process: a high voltage supply, a capillary tube with a pipette or needle of small diameter, and a conducting collector which is usually grounded. A strong electric field is generated between the tip of the needle containing the polymer pendant drop and the collector.

The precursor of the electrospinning process is a pendant drop of polymer solution. This droplet is suspended at the tip of the needle and is supported by surface tension forces. This droplet is subjected to an electric field which induces a charge on the surface of the solution. Mutual charge repulsion and the attraction between the charged droplet surface and the collector cause a force that acts against the surface tension. As the intensity of the electric field is increased, the hemispherical surface of the fluid at the tip of the capillary tube elongates to form a conical shape known as the Taylor cone [Taylor (1969)]. Further increasing the electric field, a critical value is attained where the repulsive electrostatic force overcomes the surface tension, and a charged jet of the fluid is ejected from the tip of the Taylor cone. This charged jet

undergoes instability and an elongation process that allows the jet to become very long and thin as it accelerates towards the grounded collector. During this process the solvent evaporates and fibers accumulate on the collector. By changing the collector design, the fibers obtained can be aligned or randomly interconnected. Generally on a stationary flat collector, a randomly interconnected web is obtained with time. A schematic diagram of electrospinning set up is shown in Figure 2.1.

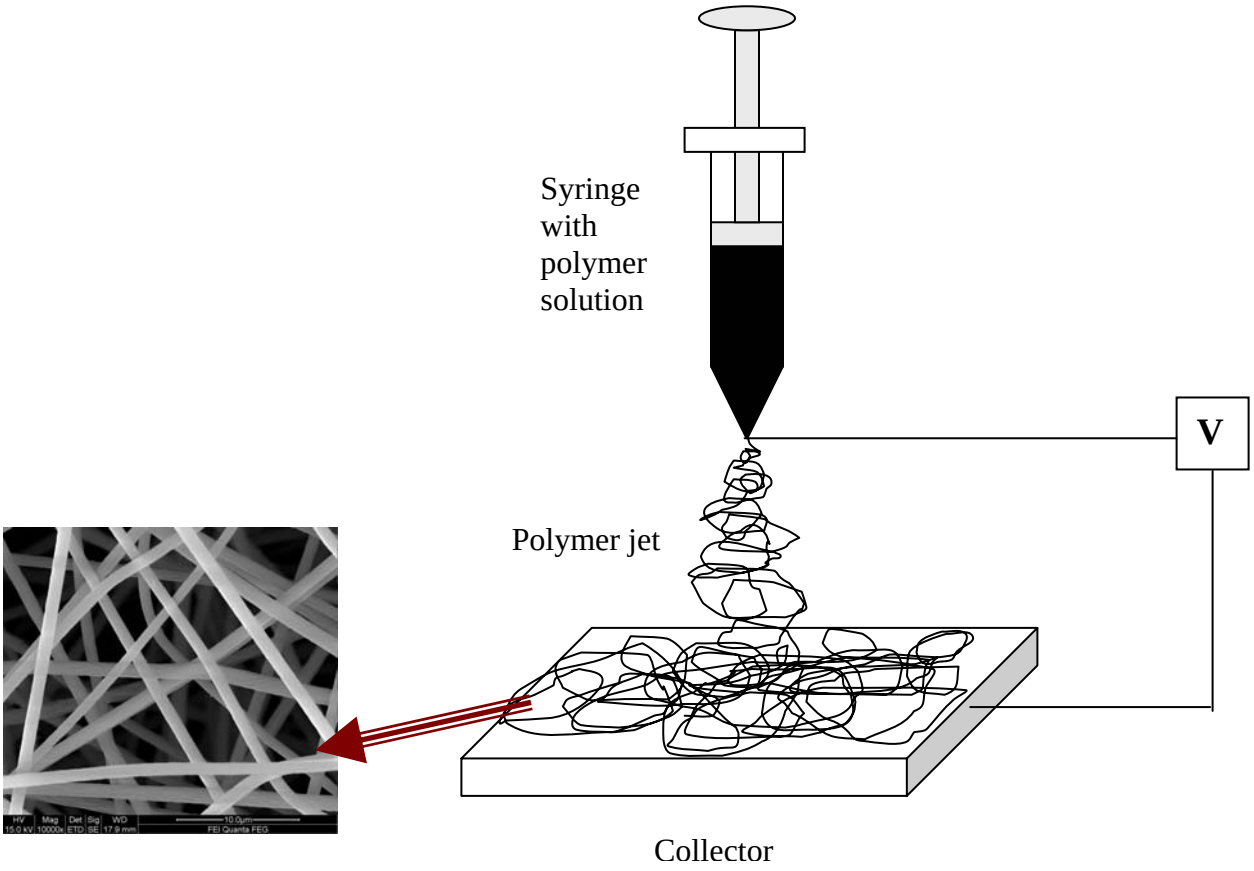

Figure 2.1: Schematic diagram of electrospinning setup

2.2 Important features of electrospinning

There are several important features of electrospinning that need to be taken into consideration. Firstly, a suitable solvent is required to dissolve the polymer and the

viscosity and surface tension of the resultant solution must neither be too large to prevent the jet from forming nor too small to allow the polymer solution to simply drain from the needle tip. The vapour pressure of the solvent should be high enough to allow quick evaporation before dry fibers are collected and not too high, such that the fibers harden before it reaches the nanometer range. The power supply should be adequate enough to overcome the viscosity and surface tension of the polymer solution to form and sustain the jet. Lastly the distance between the needle tip and the grounded collector should not be too small to create sparks between the electrodes but should be sufficiently large enough for the solvent to evaporate in time for the fibers to form. If this distance becomes too large, the fibers tend to 'fly' all over the place rather then being collected only on the grounded surface [Suthar (2001)].

2.3 Parameters affecting electrospinning

There are several parameters that affect the formation of fibers from the polymer solutions and are briefly summarized in Figure 2.2. It is also these same parameters that affect the size and type of fibers (ribbon, porous, beaded) formed. These factors can be basically categorized into three different areas, namely solution properties, processing conditions and ambient conditions. Each of these categories is influenced by several other factors where each parameter is closely related to each other. For example, changes in polymer concentration, molecular weight and solvent composition affects solution viscosity [Huang (2003)].

These set of parameters influence the formation of various polymer fibers differently. One set of processing conditions of a particular polymer cannot be used for another polymer. Hence the processing parameters have to be optimized for each polymer. In fact, it is the solution properties that are studied first for a particular polymer and it plays the most significant part in the electrospinning process and hence will be explained briefly in the following section.

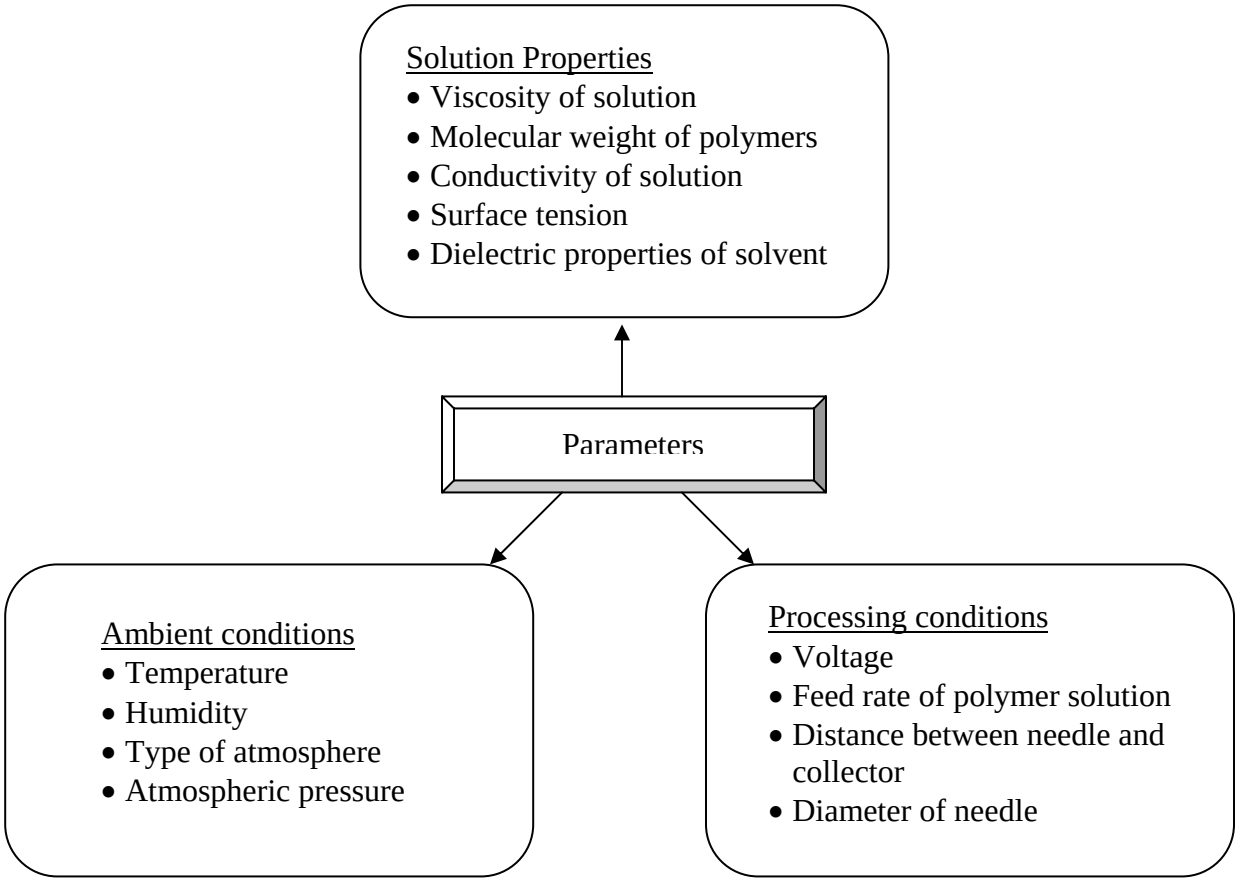

Figure 2.2: Parameters that influence the electrospinning process

2.3.1 Effect of solution properties

During the electrospinning process, the polymer solution will be drawn from the tip of the needle. The electrical property of the solution, surface tension and viscosity will determine the amount of stretching of the solution. The rate of evaporation will also have an influence on the viscosity of the solution as it is being stretched. The solubility of the polymer in the solvent not only determines the viscosity of the solution but also the types of polymer that can be mixed together [Seeram (2005)]. One of the criteria of electrospinning is that the solution must consist of polymer of sufficient molecular weight and the solution must be of sufficient viscosity. A higher viscosity is associated with a greater interaction between the solvent and polymer molecules thus when the solution is stretched under the influence of the charges, the solvent molecules will tend to spread over the entangled polymer molecules thus reducing the tendency for the solvent molecules to come together under the influence of surface tension. The applied charges on the polymer solution must be high enough to overcome the surface tension of the solution. Surface tension has the effect of decreasing the surface area per unit mass of a fluid. As the jet accelerates from the tip of the needle to the collector, the solution is stretched. During the stretching of the polymer solution, it is the entanglement of the molecule chains that prevents the electrically driven jet from breaking up thus maintaining a continuous solution jet. If the viscosity is not high enough then the surface tension of the solution may cause the solution to breakup into droplets and this process is called electrospraying [Morozov (1998), Christanti (2001), Shummer, (1983)]. Surface tension has also been attributed to the formation of beads on the elecrospun fibers. Surface tension of a polymer

solution can be reduced by employing solvents such as ethanol [Fong (1999)] which has low surface tension or adding surfactants to the solution [Zeng (2003)].

A solution with high conductivity is preferred as the overall conductivity of the solution is increased more charges are carried by the electrospinning jet. Hence this leads to an increase in stretching of the solution in turn leading to the formation of thinner fibers. The conductivity of the solution can be increased by the addition of ions. Ad the conductivity of the solution increases, the critical voltage for electrospinning to occur is also reduced [Son (2004)]. Another effect of the increased charges is that it results in greater bending instability. As a result, the deposition area of the fibers is increased. This will also favor the formation of finer fibers since the jet path is now increased [Choi (2004)]. However, the addition of ionic salt may cause an increase in the viscosity of the solution. Thus although the conductivity of the solution is improved, the viscoelastic force is stronger than the columbic force resulting in an increased in the fiber diameter instead [Mit-uppatham (2004)].

Solvents with greater dielectric property are usually employed to improve the fiber morphology. Similar to the effect of higher conductivity, the bending instability of the electrospinning jet also increases with higher dielectric constant and hence facilitates the reduction of the fiber diameter [Hsu (2004)]. However the interaction between the solvent and the polymer will also have an impact on the morphology of the resultant fibers. For example, when a high dielectric solvent N,N-Dimethylformamide (DMF) was added to polystyrene solution, beaded fibers were generated. This could be the

result of the retraction of PS molecule due to poor interaction between PS and solvent molecules [Wannatong (2004)].

2.4 Motivation I

Producing polymer fibers on the nanoscale through electrospinning requires the optimization of several parameters. Hence Chapter 3 would be dedicated in optimizing the conditions in generating nanofibers. The influence on some of the processing conditions, molecular weight, solvent, concentration and feed rate on the selected material for this thesis would be studied.

2.5 Applications of ENMs

The electrospun mat produced possesses attractive properties such as high porosity, high spatial interconnectivity, high surface area for capturing or functionalization of specific chemical groups, high permeability for gases and controllable mesh thickness [Huang (2003)]. These attributes make them highly attractive in separation technology and they have been highly successful in high performance air filters [Tsai (2002), Graham (2002)]. The high surface area of the fiber mesh produces an extremely effective removal of the airborne particles by both physical trapping and physical adsorption [Gibson (2001), Timothy (2003)]. Industrial giants like Donaldson Inc, sell nanofiber incorporated air filter products. Filtration efficiency is closely related to fiber fineness and thin fibers can be obtained through electrospinning. In addition to air filtration, electrospun articles have been demonstrated in many other applications such as tissue engineering [Zuwei (2005a),

Zuwei (2005b), Yoshimoto (2003), Shin (2004), Xu (2004)], drug deliver carrier [Luu YK (2003), Geert (2003)], biosensor/chemosensor [Wang (2002), Gouma (2003)], electronic and semi-conductive materials [Choi (2003), Caruso (2001)], reinforced nanocomposites [Bergshoef (1999)]. However their use in liquid separation is rather limited and still in its infancy [Wang (2005), Yoon (2006)]. The application of ENMs has yet to make similar break-through in pressure driven liquid separation as micro (MF), ultra (UF) or nano (NF) filters.

Motivation II

Presently, no study has been done on the ENMs on their liquid separation efficiency. Attractive attributes of ENMs such as high porosity, high spatial interconnectivity and high surface area can be capitalized for liquid separation to develop a high flux membrane. An attempt would be made to develop a complete self-supporting membrane through electrospinning. A particle challenge test will be performed on the as-spun ENMs to evaluate its separation characteristics. It is anticipated that through surface modification the surface pores will be reduced and hence the membrane will be capable of separating smaller sized particles. In this light, the surface of the ENMs would be modified to generate a ‘tighter’ MF ENM.

2.7 Membranes for liquid separation

2.7.1 Definition of a membrane

A membrane acts as a selective boundary between two phases (phase 1 and 2) that restrict/permit the passage of certain chemical species in a very specific manner (Figure 2.3). Species migrate from phase 1 to phase 2 under the influence of a driving force. Phase 1 is called as the feed while phase 2 is considered permeate. The species left behind on the fed side is called the retentate.

A membrane can be homogenous or heterogeneous, symmetric or asymmetric in structure, it may be a solid or liquid, it may be neutral, may carry positive or negative charges, or may be bipolar. Its thickness may vary between less than 100nm to more than a centimeter [Mark (1990)]. In many cases, membrane separation processes are faster, more efficient and more economical than conventional separation techniques [Nunes (2001)].

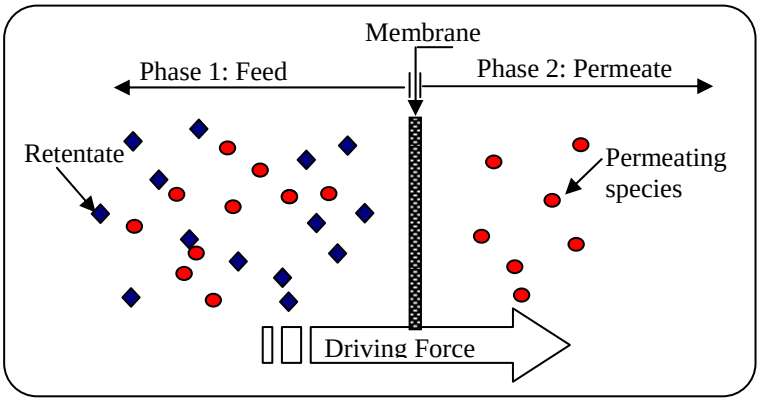

Figure 2.3: Schematic representation of a membrane

2.7.2 Classification of membranes

Membranes can be classified into two categories namely biological or synthetic (Figure 2.4). Biological membranes are essential to life and every living cell is surrounded by a membrane. However these membranes differ completely from synthetic membranes. They are highly complex, with a characteristic basic lipid bilayer structure. Synthetic membranes on the other hand are simple in structure. These membranes can be organic (polymeric), inorganic (ceramic) or a composite. All industrial applications rely on synthetic membranes [Mulder (1996)].

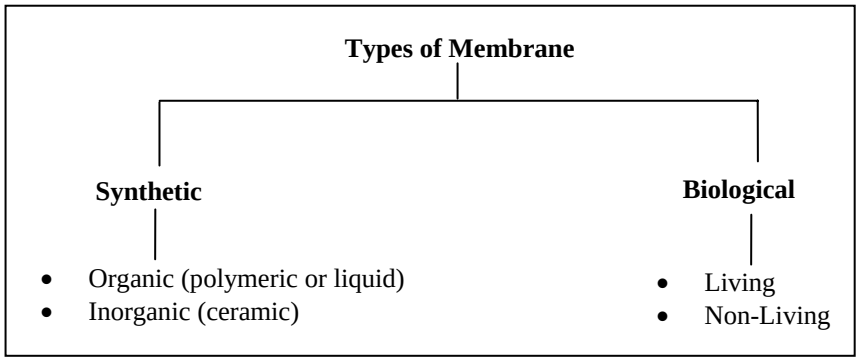

Figure 2.4: Flow chart of types of membranes

2.7.3 Properties of a membrane

2.7.3.1 Selectivity and flux

The performance or efficiency of membrane processes is governed by 2 factors: Selectivity or retention and flux (flow of permeation rate) through the membrane. Selectivity is a measure of the relative permeation rates of different components through a membrane while retention is the fraction of solute in the feed retained by

the membrane. Flux however, is governed by how much gets into the membrane (solubility) and how fast it moves (diffusivity). It is defined as the volume flowing through the membrane, per unit area and time. A membrane with a high selectivity or retention and with a high flux or permeability is desired, although attempts to maximize one factor results in the reduction of the other [Mark (1990)].

2.7.3.2 Pore-size, pore-size distribution and porosity

Pore-size refers to the diameter of the pores present in the membrane. Such information can discriminate between the type (size or molecular weight) of species that can permeate through and that will be retained. It is also common to provide the molecular weight cut off rating in place of the pore size.

However, pores in membrane, especially polymeric membrane, do not all have identical pore-size but rather a range of sizes. This is known as the pore-size distribution. Whereas, porosity is the fraction of the membrane volume occupied by the pores (empty space volume). While the pore size and its distribution discriminates the type of species that can permeate, it is the porosity that determines the flux.

2.7.3.3 Concentration polarization and fouling

In membrane processes, almost always there is a drop in flux over time. This is due to the build up of resistance to the flow of permeate. The extent of the drop is very much dependent on the type of process. This is mainly attributed to concentration

polarization and fouling of the membrane. It is very prominent in porous membranes that separate based on size-exclusion principle.

As the membrane selectively removes one component from the feed solution, there will be an accumulation of retained molecules near the membrane surface. Thus, as more permeate is removed, the retentate concentration increases several folds on the membrane surface. This forms a resistive layer hindering the mass-flow across the membrane. This is called concentration polarization. This phenomenon unfortunately is inherent to membrane processes. However, it is a reversible phenomenon that can be removed if the feed solution is continuously agitated to maintain uniform concentration profile.

In some instances, even when maintaining a fairly uniform concentration profile there is a significant drop in flux. This is then due to membrane fouling. Fouling refers to the reversible/irreversible deposition of retained particles on or in the membrane. Once again this is especially prominent in porous membranes. It is usually much more difficult to reduce fouling in a membrane as it depends on many parameters [Fane (1987)].

2.7.4 Membrane structure

Another means of classifying membranes is by morphology or structure. Membrane structure is very important as it dictates not only the separation and permeation mechanism but as a consequent the application as well. Restricting to synthetic (solid)

membranes, two types of membrane structures may be distinguished: symmetric and asymmetric membranes.

2.7.4.1 Symmetric membrane

A membrane having the same chemical and physical structure throughout is called a symmetric membrane. The thickness of symmetric membranes (porous or nonporous), range roughly from 10-200 μm. The resistance to mass transfer is determined by the total membrane thickness. A decrease in membrane thickness results in an increased permeation rate. Thus for such membranes, the top surface determines the nature of separation and the thickness governs the rate of the process.

2.7.4.2 Asymmetric membrane

Asymmetric (aniosotropic) membrane is a membrane with different chemical and/or physical structures in the direction of its thickness. It was asymmetric membranes that made a breakthrough to industrial applications [Loeb (1962)]. It is characterized by a thin “skin” on the surface of the membrane with a thickness of 0.1 to 0.5 μm. This dense layer is supported by a porous structure with thickness of 50 to 150 μm. A composite membrane comprising of more than one material are also asymmetric membranes. The top and sub layer originate from different polymeric materials. The top is a thin dense polymer skin formed over a microporous support film. Each layer can be optimized independently.

Due to its unique ultrastructure, rejection only occurs at the surface and retained particles do not enter the main body of the membrane. As such, these asymmetric membranes rarely get “plugged”. The resistance to mass transfer is determined largely by the thin top layer. The support layer does not add any significant hydraulic resistance to the flow of solvent through the membrane [Klein (1991)].

The dense layer on the support layer can be achieved by various methods such as dip-coating, interfacial polymerization, in-situ polymerization or plasma polymerization. Usually the top layer is the active layer made up of high performance polymer that causes the separation of the solutes. This layer has a thickness around 0.15 to 1 μm. This layer on its own has insufficient mechanical strength and requires some support/reinforcement. The resultant membrane formed after modification is termed as a composite membrane. As such, the desirable reinforcement material has to be porous with desirable mechanical properties and should not resist the passage of liquid.

The use of reinforcement has several advantages: it reduces cost; increases the ratios of strength to density and stiffness to density; increases resistance to corrosion, fatigue, creep, and stress rupture; and reduces the coefficient of thermal rupture. Reinforcements allow the material to be tailored to the design, instead of the design being tailored to the material [Kroschwitz (1990)]. Both symmetric and asymmetric membranes can be further classified as shown in the Figure 2.5.

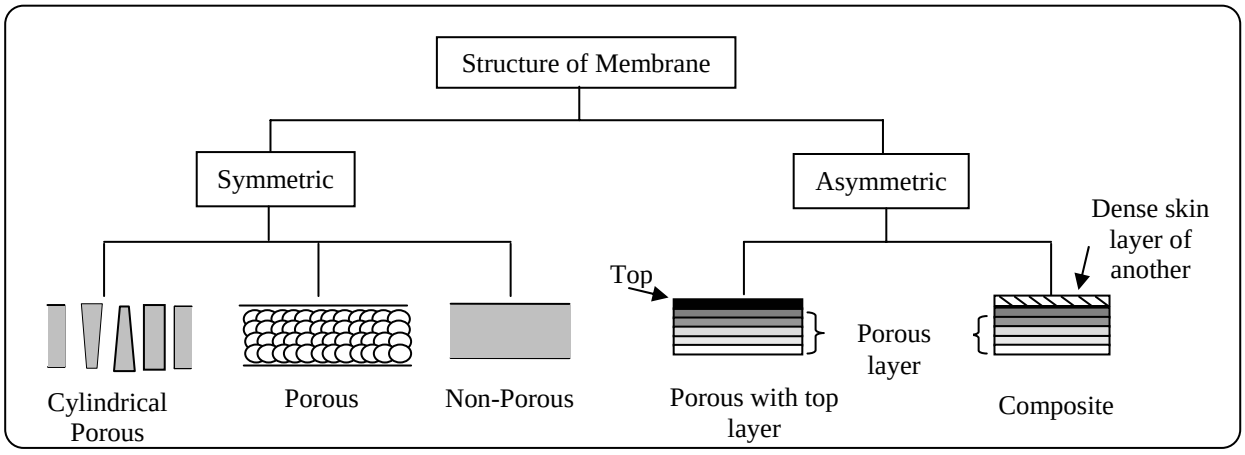

Figure 2.5: Classification based on structure of membrane

2.7.5 Driving Force

A driving force is essential for the transport of species across a membrane. The transport through the membrane only occurs when a driving force is applied on the individual components in the feed solution. The flux is determined by the driving force acting on the permeating species and their mobility and concentration within the interphase [Strathmann (1981)]. There are four different categories of driving forces, namely, pressure, temperature, concentration and electric potential differences across the membrane [Matsuura (1994)]. This is reflected in Table 2.1.

Driving force across the membrane	Processes
Pressure Difference	Microfiltration (MF)
	Ultrafiltration (UF)
	Reverse Osmosis (RO)
	Nanofiltration (NF)
	Gas Separation
	Pervaporation
	Piezodialysis
Temperature Difference	Membrane Distillation
Concentration Difference	Dialysis
Electric Potential Difference	Electrodialysis

Table 2.1: Driving forces across a membrane

As-spun ENMs are classified as microfiltration membranes [Gopal (2006)] and hence information on only this class of membrane will be mentioned in this thesis.

2.7.5.1 Microfiltration (MF) membrane

MF membrane is a porous membrane and has the largest pore diameter among all the pressure driven membranes shown in Table 2.1. The pressure applied across the membrane is about 1 to 2 bars and is applied to the feed side of liquid during operation. The osmotic pressure is negligible. The selective layer thickness is in the range of 10-150 μm [Mulder (1996)]. The membrane structure is usually symmetric. MF membrane can separate microparticles with diameters of about 0.03 to 10 μm. Colibacillus and staphylococcus are two examples of microparticles which can be

removed by such a membrane. In other words, MF membranes are permeable to all dissolved species. They retain no solutes (except by adsorption) but retain particles, including colloidal particles. If particles do get adsorbed onto the surface of the pore, the pore size gets reduced significantly. Particles can also be deposited on top of the membrane, forming a cake-like secondary filter layer. MF is used in several industries like fermentation, medical, electronic and food and beverage [Toyomoto (1992)].

2.7.5.2 Methods of MF manufacture

A number of techniques exist for preparing microfiltration membranes. They are sintering, stretching, track etching and phase inversion. These techniques are not generally used to prepare UF membranes because the pore sizes obtained are only in the MF range except for the case of phase inversion [Mulder (1996)].

If the thickness of the fibrous mat formed during electrospinning is controlled, a MF membrane can be formed as well. Through electrospinning, a highly porous membrane can be obtained and hence this will lead to a higher flux. However the membrane obtained through electrospinning is symmetric and this is reflected in Figure 2.6. In addition to this the membranes formed through electrospinning have large pores and hence classified as ‘loose’ microfiltration membranes (Figure 2.7). As indicated by the arrows in Figure 2.7, the surface pore sizes are between 5 to 10 µm. Having an interconnected fibrous structure the overall pore sizes of the ENMs are definitely reduced but the extent of reduction remains unknown. The technique limits

the usage of electrospun membranes for separation of even smaller particles. To utilize the important and useful characteristics which electrospinning offers, the surface of the as spun membranes should be subjected to treatments so as to generate a 'tighter' MF membrane.

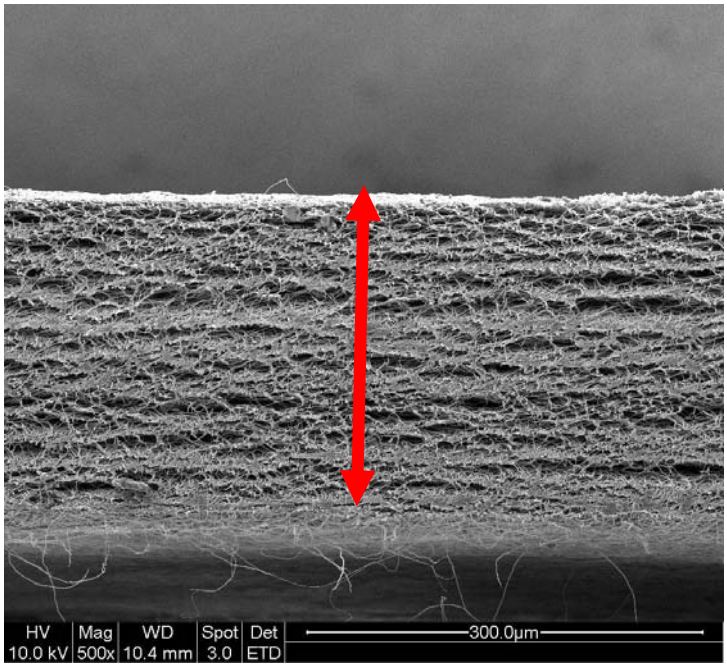

Figure 2.6: Cross section of ENM revealing a symmetric structure. The arrow indicates a uniform cross section of the ENM.

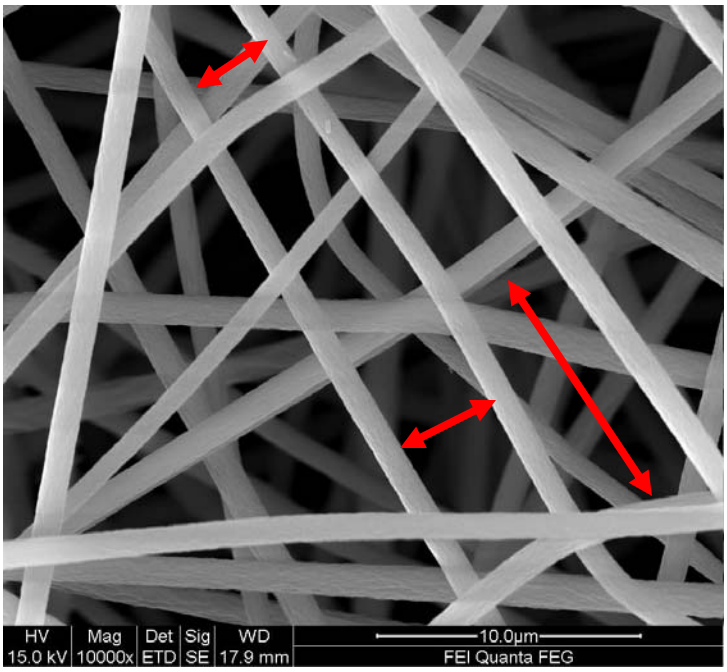

Figure 2.7: SEM micrograph of a typical ENM. Arrows are drawn to indicate the large air pockets.

2.8 Surface modification

The main purpose of surface modification is to alter surfaces by either chemically or physically altering the atoms/molecules in the existing surface, changing the surface topography or coating over the existing surface with a material having a new composition [Penn (1994), Chan (1996), Kato (2003)] to meet a specific requirement or application.

The polymers generally used to fabricate MF membranes are hydrophobic [Mulder (1996)]. However a hydrophobic surface has an increased adsorption tendency. The adsorption of solutes has a negative influence on the flux because the adsorbed layer presents an extra resistance towards mass transfer and consequently contributes to a decline in flux. In addition, adsorption layers are difficult to remove by cleaning

methods. Although hydrophilic polymers such as cellulose and its derivate have been utilized as MF membranes, these classes of polymers are sensitive to thermal, chemical and biological degradation. Hence using such hydrophilic polymers to make the bulk of the membrane is not preferred [Nunes (2001)].

Generally a thin hydrophilic layer is introduced on the surface of the base hydrophobic membrane. Surface modification is employed to change the surface chemistry of the base membrane so as to improve the flux. In addition to this, another advantage of surface modification is that it can change the surface physically where the surface pores are reduced.

2.8.1 Factors to be considered when modifying a surface

There are a few factors to be considered when modifying a surface [Wu (1982), Griesser (1990), Gupta (2002)] of a membrane:

i. Thickness of the surface is crucial. Thin surface modifications are desirable otherwise mechanical and functional properties of the material will be altered and an overall thicker membrane results in a lowering of flux.

ii. Sufficient atomic or molecular mobility must exist for surface changes to occur in reasonable periods of time. The driving force for the surface changes is the minimization of the interfacial energy.

iii. Stability of the altered surface is essential, achieved by preventing any reversible reaction. This can be done so by cross-linking and/or incorporating bulky groups to prevent surface structures from moving.

iv. Uniformity, reproducibility, stability, process control, speed and reasonable cost should be considered in the overall process of surface modification.

2.8.2 Surface modification techniques

Common surface modification techniques used on polymer substrates include treatments by blending, coating, surface segregation, layer by layer electrostatic interaction, radiation of electromagnetic waves, electron beam, ion beam [Dong (1999), Brown (1993)] or atom beams [Chan (1996)], corona or plasmas treatment [Liston (1993), Grace (2003), Chu (2002)], chemical vapor deposition (CVD), gas oxidation, metallization, chemical modifications using wet-treatment and surface grafting polymerization [Uyama (1998), Kato (2003)] etc. In recent years, many advances have been made in developing surface treatments to alter the chemical and physical properties of polymer surfaces and progress in recent years has been summarized in many reviews [Ratner (1995), Ikada (1994), Desai (2004)].

Of the above mentioned techniques, only blending, grafting, plasma induced grafting and plasma treatment have been utilized to date on nanofibers with success. One of the simplest methods of surface modification is to introduce surfactants [Kaur (2006), Ramaseshan (2006)] into the polymer solution before electrospinning. However, the blending method in electrospinning, introduces the surfactants throughout the membrane and not on the surface of the membrane. Blending in electrospinning will not reduce the overall pore size of the electrospun membrane but instead it may produce larger pores as it may affect the packing orientation of the

fibers. An ultrafiltration (UF) based ENM has been developed by introducing a coating layer on the surface of the ENM [Wang (2005), Yoon (2006)]. Affinity membranes and scaffolds for tissue engineering have been developed through grafting [Hong (2005)] and plasma induced grafting [Chua (2004), Ma (2006a), Ma (2006b) Zuwei (2005)]. Plasma treatment on the other hand changes the surface properties such as hydrophilicity. However, the plasma treatment effect does not reduce the pore size significantly and can be time dependent resulting in "hydrophobic recovery". To retain permanent long term hydrophilicity as well as a reduction in pore size, the plasma treated surface is subjected to further modification such as surface graft co-polymerization [Wavhal (2003)].

2.8.2.1 Plasma induced graft copolymerization

Plasma-induced graft co-polymerization treatment is limited only to the surface and hence the bulk properties of the membranes are still maintained. It is a versatile method usually employed to introduce groups to improve the hydrophilic chemistry so as to fine tune the separation characteristics of the membrane such as the reduction of fouling. In addition to this pore reduction can be achieved at the surface with cross-linking with another polymer or deposition of a thin selective layer on a porous substrate. If the time of the exposure is optimized, a controlled reduction of pore size can be obtained and a MF membrane can be transformed into an UF or even RO membrane [Nunes (2001)].

The surface of the membrane is initially exposed to plasma. Plasma is a complex gaseous state of matter, consisting of free radicals, electrons, photons and ions. Plasma can be generated by continuous electrical discharge (glow discharge or corona discharge) in either an inert or a reactive gas [Chatelier (1995), France (1998), Cen (2003), Kou (2003), Suzuki (1986), Clouet (1992), Bryjak (2001), Osada (1986), Iwata (1991), Wang (2002), Wavhal (2002)]. This is then followed by exposure of the activated surface to oxygen to form peroxides. This membrane is then heated with a desired unsaturated monomer to form polymer chains on the surface.

2.9 Motivation III

It is anticipated that as-spun ENMs are only able to separate microparticles of a larger range but to what extent? To answer this question a particle challenge test will be performed on the as-spun membranes. Since the as-spun ENMs are only able to separate larger microparticles, an attempt would be made to modify the surface of the as spun ENMs through plasma induced graft polymerization to achieve a high flux asymmetric microfiltration ENM. A water flux permeation, pore-size and pore-size distribution comparison would be made between the surface modified ENM and a commercial membrane. This would surface the usefulness of ENMs in the field of membrane science. This thesis will open up avenues of using ENMs for separation technology.

Chapter 3

Material Selection and Electrospinning

3.1 Membrane requirement

Selecting the right material is very critical in separation technology. It is important to understand the influence of a material's intrinsic properties to the separation mechanism.

By far the most versatile group of materials for membrane synthesis is polymers. Polymers can be tailored to meet specific requirements such as mechanical, thermal, hydraulic, chemical stability and high biodegradability. However, the chemical and physical properties differ so much that only few have achieved commercial status [Kroschwitz (1990)].

The selection of a material for a certain application involves different criteria. For a porous MF membrane, the choice of the material does not directly determine the separation characteristics since the pore-size and the pore-size distribution are the main factors influencing the separation of particles. However the choice of polymer definitely affects the chemical and thermal stability and surface characteristics such as adsorption and wettability [Mulder (1996)]. Additionally the choice of polymer is crucial when certain cleaning agents are employed. For example polyamides are strongly attacked by chlorine-containing cleaning agents and hence should not be selected when such as agents are required for sterilizations. The materials of MF

generally consist of crystalline polymer generally engineering plastics including cellulose and its derivatives. Hydrophilic materials are not suitable for MF membranes that require mechanical strength and thermal stability [Toyomoto (1992)].

Hydrophobic materials such as polytetrafluorethylene (PTFE), poly(vinylidene fluoride) (PVDF) and isotactic polypropylene (PP) are often used for MF membranes. PTFE is highly crystalline and possesses excellent thermal stability and is chemically resistance. Because of its chemical inertness, this polymer was not chosen to be electrospun since one of the requirements of electrospinning is to dissolve the polymer in a suitable solvent. Similarly PP is an excellent solvent resistant polymer and hence not suitable to be subjected to electrospinning. On the other hand PVDF exhibits good thermal and mechanical properties. In addition to this, it is chemically resistant but it is soluble in aprotic solvents such as N,N-dimethylformamide (DMF) and N,N-dimethylacetamide (DMAC). Because of its good solubility in solvents that possess a high dielectric constant and its resistance to severe environmental stresses, PVDF has been selected for this research work to be electrospun into a MF membrane. The membrane generated is generally hydrophobic and surface modification would provide a means to generate a hydrophilic surface as well as reducing surface pore size.

3.2 Electrospinning of Poly(vinylidene fluoride)

3.2.1 Methadology

The electrospinning set up used for this research work is shown in Figure 3.1. The essential materials are the syringe pump, syringe and needle, conductive collector that is grounded and a dehumidifier. The syringe pump (New Era Pump Systems Inc, USA, Ne-1000) held the syringe that was connected to a needle. The feed rate of the polymer solution is controlled by the syringe pump and was varied between 1 to 16 ml/hr depending on the experimental plan. The needle tip was clamped with a crocodile clip connected to a high voltage regulated DC power supply (RR 50-1.25R/230/DDPM, GAMMA, high voltage research, USA). The humidity level in the fumehood was around 90% and was rather high. A high humidity usually affects the solvent evaporation rate and hence affects the formation of fibers. Hence the humidity was reduced to approximately around 70 % by using a dehumidifier. The voltage was increased slowly until a jet formation was observed. A voltage of 15 kV was observed to be suitable for the solutions that were easily electrospun. The distance between the needle tip and collector was fixed at 15 cm. The collector was an aluminum plate with a 10 cm by 10 cm dimension and was grounded. The thickness of the electrospun membrane can be varied by increasing the collection time. After the electrospinning process, the electrospun membrane was placed in a vacuum oven at 30^0C overnight to remove any residual solvents before any characterization was performed.

The thickness of the heat treated membrane was measured using a micrometer screw gauge (Mitutoyo, Japan). The morphology of the ENMs was observed using a field-emission scanning electron microscope (FESEM) (Quanta 200F, FEI, Netherlands). The membranes were mounted on the sample studs by means of double sided conducting adhesive tapes and were sputtered with gold prior to SEM measurements. Coated samples were examined at an accelerating voltage of 10 kV. The diameter of the fibers was determined using the ImageJ software (http://rsb.info.nih.gov/ij/) and 50 counts were taken for each condition from different SEM micrographs.

3.2.2 Influence of electrospinning parameters on fiber morphology

As mentioned in the literature review, there are several factors that influence the formation of fibers and their morphology during electrospinning. Changing the concentration, molecular weight, solvent and humidity level can lead to different morphology such as thin or fat fiber, branched fibers, flat ribbons, beaded fibers and last but not least, porous fibers [Casper (2004), Bognitzki (2001), Koombhongse, (2001), Fong (1999)]. However not all the parameters are the same for every polymer. Hence the electrospinning conditions have to be optimized for a particular polymer. The influence of factors such as molecular weight, solvent, concentration, feed rate and collector type on the formation and morphology of the PVDF nanofiber were studied.

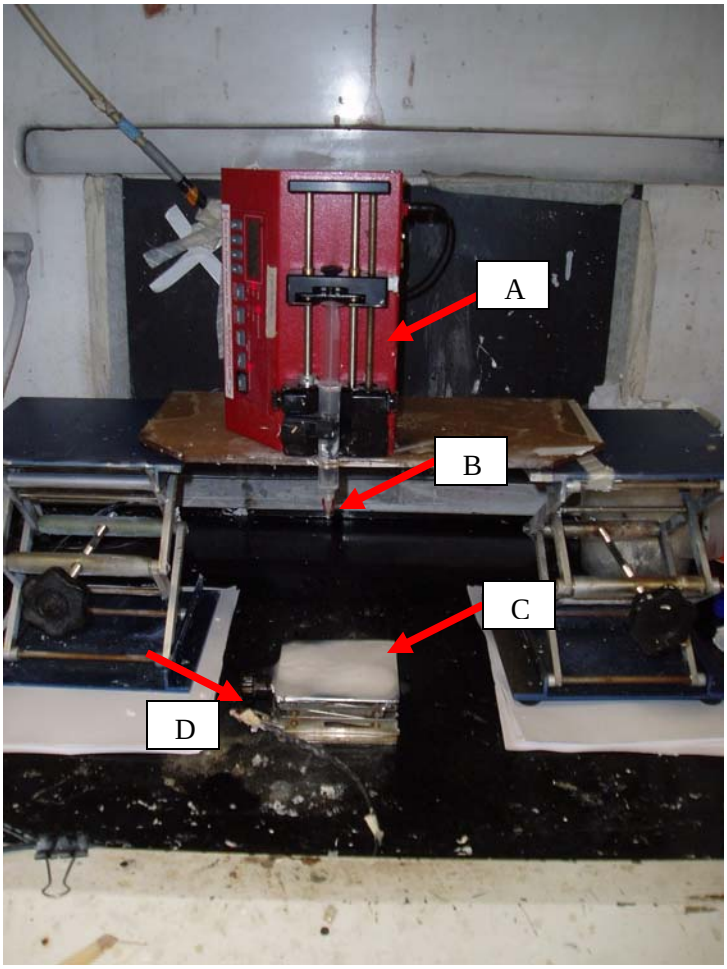

A= Syringe Pump
B= Needle attached to a syringe. A crocodile clip that is connected to the high voltage supply is clamped at the tip of the needle
C= Collecter
D= Crocodile clip that is grounded

Figure 3.1: Electrospinning set up used to generate ENMs

3.2.2.1 Effect of molecular weight

The first step of optimization of the electrospinning of PVDF was to select the most suitable molecular weight. It is known that PVDF has a high solubility in solvents such as DMAC, DMF, 1-methyl-2-pyrrolidinone (NMP) and mild solubility in acetone (AC). Hence four different molecular weight (MW), 180 000, 275 000, 440 000, 530 000 g/mol of PVDF were initially dissolved in DMAC, with a concentration range of 0.1 to 0.25 g/ml and electrospun. The voltage was fixed at 15kV.

In order for electrospinning to occur, a certain amount of solution viscosity is required. At a very low concentration, the solution containing MW 180 000 and 275 000 g/mol was not visibily viscous and resulted in sputtering. When the concentration was raised to 0.25 g/ml, fibers were not formed as well. MW affects the viscosity of the solution. The lower the MW, the lower the viscosity of the polymer solution even if the concentration is increased. When the polymeric MW is low, there is less entanglement of the polymer chains and hence destabilizing the electrically driven jet resulting in electrospraying rather than electrospinning. Hence the MW 180 000 and 275 000 g/mol were not suitable for further optimization.

On the other hand the polymer solution containing MW 530 000 g/mol was considerably viscous even at a lower concentration of 0.1 g/ml and it resulted in occasional blockage at the tip of the needle. It was also very difficult to pump the highly viscous solution through the syringe connected to a needle with a small bore. In order to overcome the blockage of the needle tip and ease of solution flow, a large bore needle could be used but this would lead to the formation of fatter fibers and optimizing other parameters to produce thinner fibers would have been rather challenging. Hence this MW was not selected for further optimization.

When the PVDF pellets with MW 440 000 g/mol were dissolved in a concentration of 0.15 g/ml in DMAC, fibers as well as beads were produced (Figure 3.2). This indicates that the concentration is not high enough, as such the concentration was raised to 0.25 g/ml. Increasing the concentration produced fatter fibers and lesser

beads. When a thick membrane layer was electrospun, the overall membrane was dissolved due to the presence of residual DMAC which has a low vapour pressure of 0.178kPa, and hence not able to evaporate fast enough before the fibers were collected. Next DMF which has an enhanced solubility for PVDF was selected to dissolve the PVDF pellets at a concentration of 0.15 g/ml. Again a similar observation with the DMAC system was made. This MW was chosen to be subjected to further optimization to produce fibers without beads in the nanometer range. It was anticipated that by further optimizing the solvent properties, beads can be avoided and fine and uniform fibers can be produced. The SEM micrographs of PVDF dissolved in DMAC at a concentration of 0.15 g/ml and 0.25 g/ml and DMF at a concentration of 0.15 g/ml is presented in Figure 3.2.

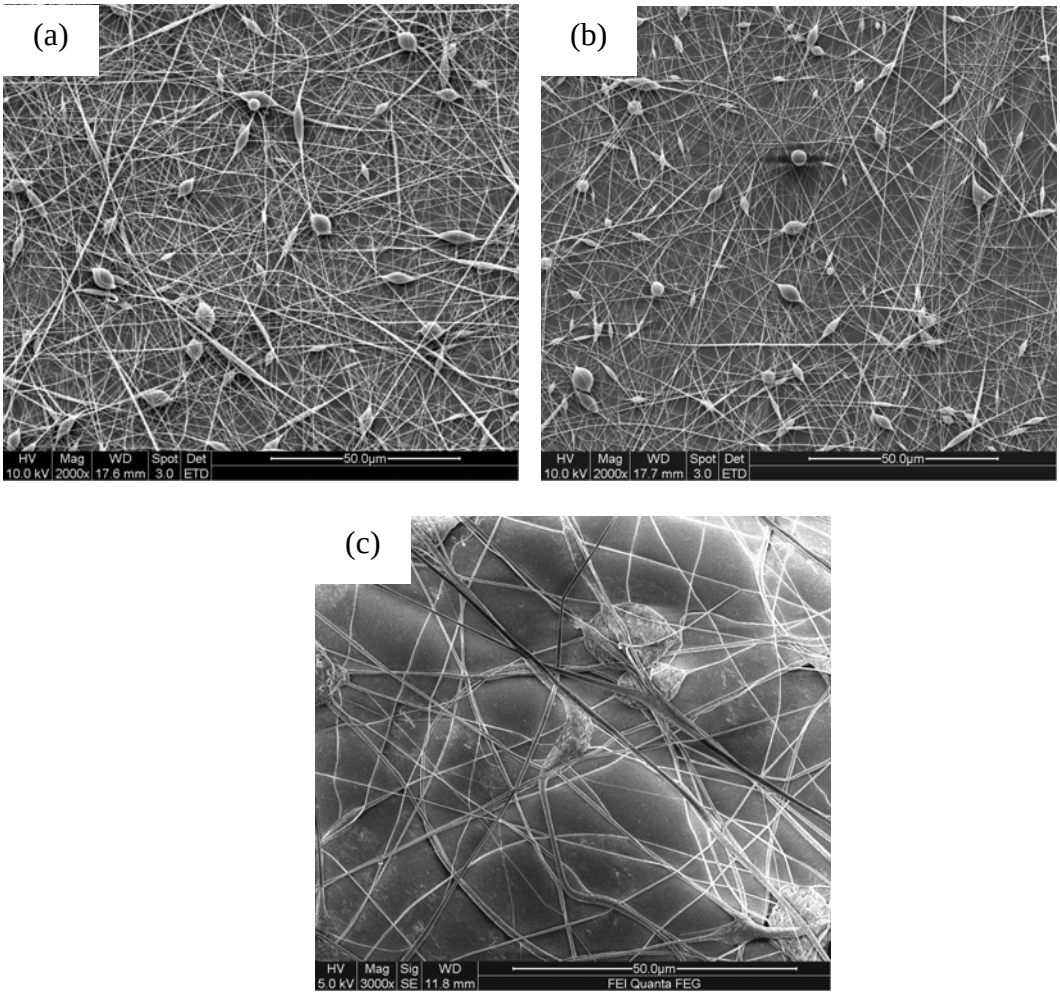

Figure 3.2: SEM micrograph of PVDF (MW: 440 000 g/mol) at a concentration of (a) 0.15 g/ml dissolved in DMAC, (b) 0.15 g/ml dissolved in DMF, (c) 0.25 g/ml dissolved in DMAC

3.2.2.2 Effect of solvent

In this section, suitable solvents were employed to electrospin PVDF of MW 440 000 g/mol. The solvents were selected on the basis of their ability to dissolve PVDF, dielectric constant, conductivity and/or vapor pressure.

Although PVDF is chemically inert it can be readily dissolved in organic solvents such as DMAC, DMF, NMP and has mild solubility in acetone. Hence these four solvent have been tested for their ability to dissolve PVDF in appropriate combinations before subjecting the polymer solution to electrospinning. In addition to this, pyridine has also been chosen to spike the polymer solution since it has been reported that pyridine improves the conductivity of the polymer solutions and hence helps to reduce bead formation [Huang (2006)]. Electrospinning involves stretching of the solution caused by repulsion of the charges at its surface. Thus if the conductivity of the solution is increased, more charges can be carried by the electrospinning jet [Seeram (2005)]. Solution prepared using solvents of higher conductivity generally yield fibers without beads while no fibers are formed if the solution has zero conductivity [Jarusuwannapoom (2005)].

To prevent the formation of a membrane with residual solvents trapped within it which ends up dissolving the fibers again, it would be desirable to use a solvent which is volatile. Volatility is associated with the liquid's boiling point or vapour pressure. Usually the higher the vapour pressure of a material at a given temperature, the lower the boiling point [http://en.wikipedia.org/wiki/Vapor_pressure]. A solvent with high volatility has a high vapor pressure and hence it would be desirable to combine DMAC with a solvent with a lower boiling point and high vapour pressure such as AC. AC has an extremely high vapour pressure of 25kPa at 20^0C which is 140 times more than DMAC at the same temperature. DMF has a relative low vapour

pressure of 0.38 kPa and hence a combination with acetone will be considered as well.

All solvents except DMF were used as received without any further purification. For DMF, the solvent was dried with molecular sieves overnight before use. The properties of the several selected solvents are shown in Table 3.1.

Solvent	**Surface tension (mN/m) at 20^0C ***	**Vapour pressure (kPa) at 20^0C**	**Dielectric constant (ε) at 25^0C**	**Boiling point (^{0}C)**
Acetone	25.2	25	20.7	56.2
DMAC	36.7	0.18	37.8	165
DMF	37.1	0.38	36.5	153
NMP	40.79	0.03	32.2	202
Pyridine	38	2	12.3	115

*[www.surface-tension.de/]

Table 3.1: Comparison of surface tension, vapour pressure, dielectric constant and boiling point of solvents used to electrospin PVDF [Seeram (2005)]

The dielectric constant of a solvent has a significant influence on electrospinning. The dielectric constant of a solvent is related to the solvent's polarity. The dipole moment increases with an increase in dielectric constant and hence the presence of more polar functional groups. A solution with a greater dielectric property reduces bead formation and the diameter of the fiber formed. Solvents such as DMF may be added to the solution to increase the dielectric property to improve the fiber morphology

[Seeram (2005)]. The bending instability of the electrospinning jet also increases with higher dielectric constant. However there are situations when the polymer solubility is so good in high dielectric solvent, beads are still formed [Wannatong (2004)]. As can be seen from Table 3.1, most of the solvents have high dielectric constants with DMF and DMAC having the highest values.

The concentration of PVDF solution was fixed at 0.15 g/ml and the PVDF pellets were dissolved in different combinations of solvents such as DMAC and AC, DMAC and DMF, DMAC and pyridine and finally NMP and AC. Heat was applied at 50^0C to dissolve the PVDF pellets in the respective solvents. It was ensured that the bottles were tightly sealed to prevent moisture from entering the system as trace amounts of water tend to precipitate the polymer. The humidity, feed rate, voltage, temperature and distance from needle tip and collector were kept constant and the conditions are reported in Table 3.2.

Electrospinning conditions	**Values**
Polymer solution concentration	0.15g/ml
Humidity	~70%
Feed rate	1ml/min
Voltage	15kV
Temperature	~ 17.9^0C
Distance from needle tip to collector	15 cm

Table 3.2: Electrospining conditions for PVDF

Solvent	Morphology
DMAC	Fibers & Beads
DMF	Fibers & Beads
DMAC: AC (80:20)	Fibers & Beads
DMAC: AC (60:40)	Fibers only
DMAC: AC (50:50)	Fibers only
DMAC: AC (40:60)	Fibers only
DMAC: AC (20:80)	Fibers only
DMF: AC (80:20)	Fibers & Beads
DMF: AC (60:40)	Fibers only
DMF: AC (50:50)	Fibers only
DMF: AC (40:60)	Fibers only
DMF: AC (20:80)	Fibers only
DMAC: DMF (80:20)	Fibers & Beads
DMAC: DMF(60:40)	Fibers & Beads
DMAC: DMF (50:50)	Fibers & Beads
DMAC: DMF (40:60)	Fibers & Beads
DMAC: DMF (20:80)	Fibers & Beads
NMP: Acetone (1:1)	Sputtering (no fibers)

Table 3.3: The morphology obtained when PVDF is dissolved in different solvent combinations. The conductivity of the solvents is also reflected

Table 3.3 reflects the type of morphology obtained with different types and amount of solvents. For the solvent combination DMAC and pyridine, DMAC was initially used

to dissolve the PVDF pellet and once dissolved, pyridine was added but it resulted in precipitation of the solution instead. Thus pyridine is not a suitable solvent for spiking the PVDF solution.

The solvent combination NMP and AC was not able to generate any fibers from the polymer solution. This can be attributed by the high surface tension of NMP, 40.79 mN/m at 20^0C. The initiation of electrospinning requires the charged solution to overcome its surface tension. Surface tension has the effect of decreasing the surface area per unit mass of a fluid. As the solution jet accelerates from the tip of the source to the collector, the solution is stretched while the surface tension of the solution may cause the solution to break up into droplets [Shummer (1983), Christanti (2001)] and this process us called electrospraying [Morozov (1998)]. Surface tension is also one of the factors that contribute to the formation of beads on the electrospun fibers. Looking back at Table 3.1, the surface tension of DMF and DMAC is also high, 37.1 and 36.7 mN/m respectively, and this could have contributed to the presence of beads as shown in the micrographs in Figure 3.2. Similarly a combination of the solvent DMF and DMAC produced fibers with beads. Despite having high dielectric constants, the DMF and DMAC combination produced beaded fibers and this shows that the surface tension property supersedes the dielectric property. Another reason for the production of beaded fibers is the viscosity which can be overcome by increasing the concentration. However by increasing the concentration, the fiber diameter increases.

On the other hand, the solvent combination of DMAC/acetone and DMF/acetone, fibers were obtained. The ratio of acetone to DMAC and acetone to DMF is varied. There are two advantages in adding acetone as a second solvent and that is it posses a low surface tension 25.2 mN/m at 20^0C and a very high vapor pressure, 140 times higher than DMAC and 66 times higher than DMF. When the ratio of acetone to DMAC and ratio of acetone to DMF was low at 20% of the total solvent volume, beads were produced. As can be seen from Table 3.3, at a low percentage of 20% beads were generated. As the percentage of acetone was increased, the beads disappeared. However increasing the ratio of acetone to 80% resulted in clogging at the needle tip since acetone tends to evaporate easily and hence the solution solidifies at the tip. Changing the needle tip frequently is not recommended and hence the solvent ratio of DMAC: AC at 20:80 v/v was not considered. The effect of increasing the percentage of acetone from 40% to 60% was investigated by performing a fiber count and distribution and this is reflected in Table 3.4 and Figure 3.4 respectively.

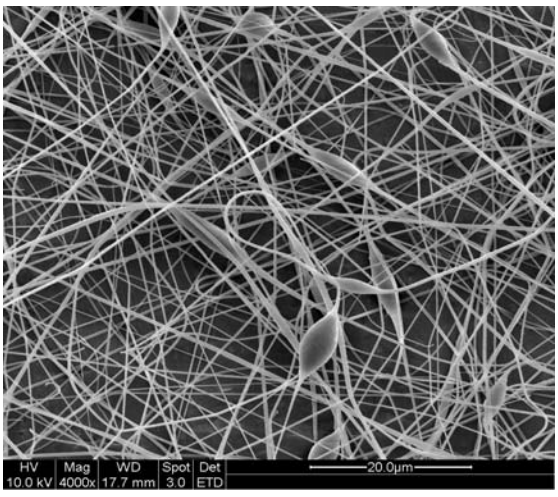

DMAC:AC (80:20 v/v)

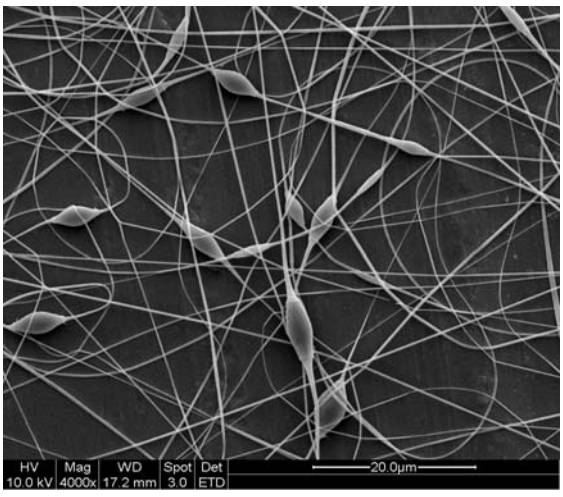

DMF: AC (80:20 v/v)

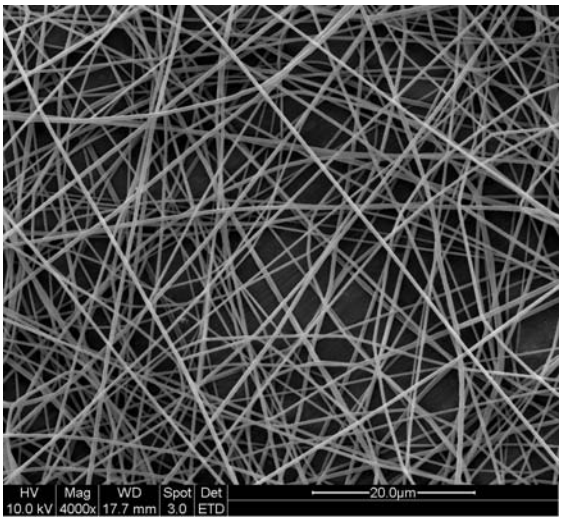

DMAC: acetone (40:60 v/v)

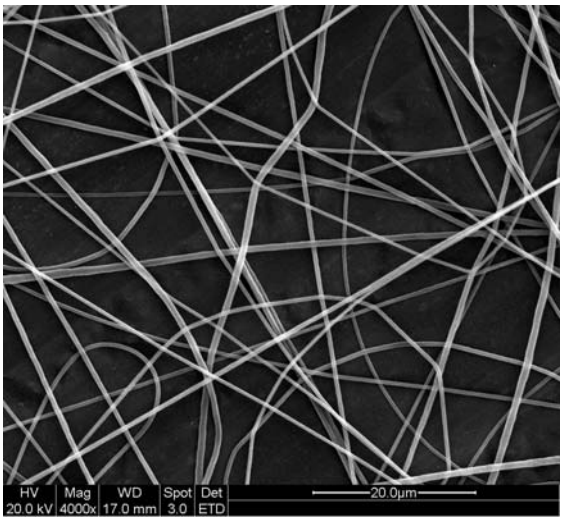

DMF: acetone (40:60 v/v)

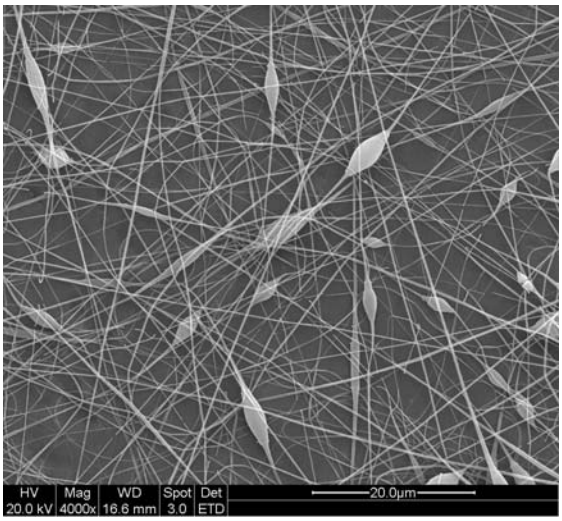

DMAC:DMF (50:50 v/v)

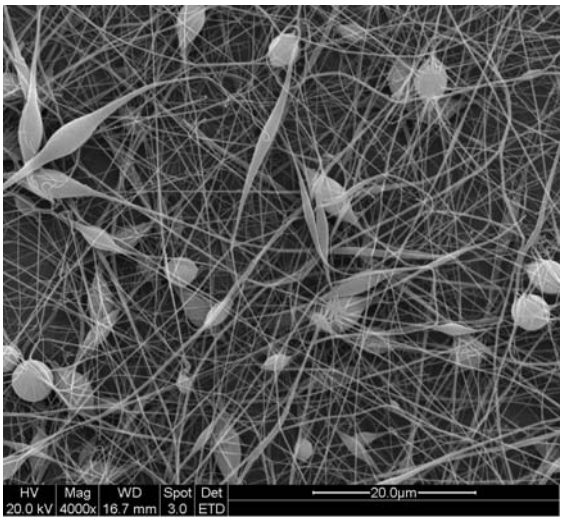

DMAC:DMF (80:20 v/v)

Figure 3.3: Effect of various types of solvent and their concentration on fiber morphology

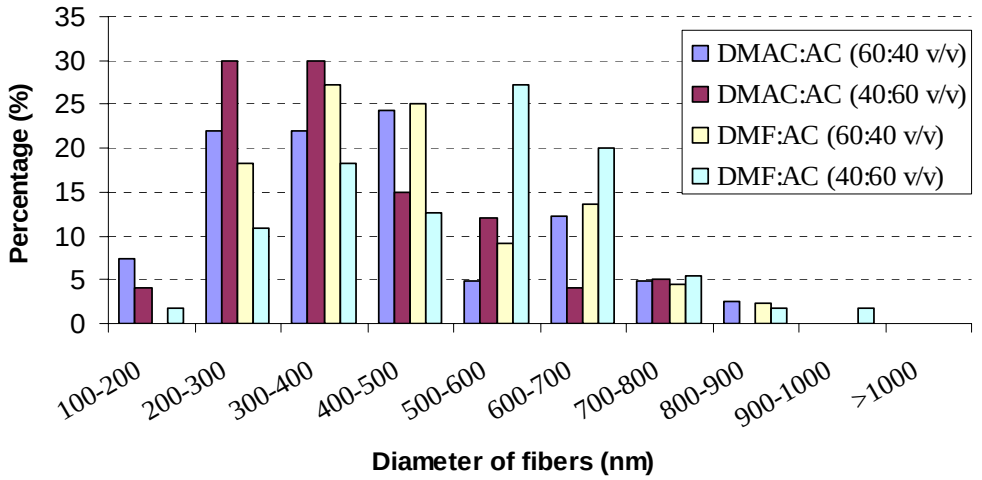

Figure 3.4: Fiber size distribution of ENM spun with different solvent combinations at a concentration of 0.15 g/ml

Solvent combination	Fiber diameter (nm)
DMAC:AC (60:40 v/v)	434 ± 198
DMAC:AC (40:60 v/v)	381 ± 147
DMF:AC (60:40 v/v)	442 ± 151
DMF:AC (40:60 v/v)	504 ± 163

Table 3.4: Average fiber size of ENM spun with different solvent combinations at a concentration of 0.15 g/ml

All four systems had a wide fiber diameter distribution from 100 to 900 nm. The system DMAC:AC (40:60 v/v) had the smallest average diameter and with narrowest fiber distribution. The system DMF:AC (40:60 v/v) had the largest average diameter of approximately 500 nm. There was not much difference in the fiber diameter for between each system. As such the system with the narrowest fiber diameter distribution, DMAC:AC (40:60 v/v) was chosen for the next step of optimization.

3.2.2.3 Effect of Concentration

In general, lowering the polymer concentration reduces the diameter of the electrospun fiber. However, lowering the concentration to a certain level gives rise to beaded nanofibers [Jaeger (1996), Fong (1999)]. Hence different concentration of the same solvent combination DMAC and acetone (40:60 v/v) was considered. PVDF concentration of 0.07g/ml, 0.09 g/ml, 0.11 g/ml, 0.13 g/ml, 0.15 g/ml, 0.17 g/ml, 0.2 g/ml and 0.25 g/ml were made and electrospun at a feed rate of 1 ml/hr.

As can be seen from the SEM micrographs in Figure 3.5, increasing the concentration of PVDF decreased the amount of beads. Interestingly, at a concentration of 0.13 g/ml, the fiber size is larger than that of 0.15 g/ml because the beads are beginning to be stretched to fiber. Beyond 0.15 g/ml no beads were observed. However the fiber diameter increases with an increase in concentration. At a concentration of 0.25 g/ml, the needle tip tends to clog. Furthermore, when a thick layer of membrane was collected, the overall mat becomes very wet as the solvent has less time to escape. A wider fiber has more solvent adhered to it as compared to a thinner fiber and hence more time will be required for most of the solvent to evaporate. As such the residual solvent surrounding the fibers tends to dissolve the fibers and hence the overall membrane was destroyed.

Changing the concentration of the polymer solution affects the viscosity of the overall solution. A minimum viscosity is required to yield fibers without beads. As can be seen from the SEM micrographs in Figure 3.5, at a low concentration of 0.07 g/ml to

0.09 g/ml, there were several beads and as the concentration was raised to 0.11 g/ml and 0.13 g/ml, the amount of beads were reduced. It was observed that the beads changed in shape from spherical at 0.07 g/ml to a spindle like shape at 0.09 g/ml, 0.11 g/ml and 0.13 g/ml. Finally, smooth fibers above a concentration of 0.15 g/ml were obtained. These observations are inline with several experiments performed on other polymeric material [Fong (1999), Mit-uppatham (2004)].

Polymer solutions have three concentration regimes, that is, the dilute regime, the semi-dilute regime and the concentrated regime. In the concentrated regime, polymer chains interpenetrate and entangle with each other, which increases the viscosity of the polymer solution. High viscosity usually favors the formation of thicker fibers without beads, but surface tension drives towards the formation of beaded fibers. Although the surface tension, which is one of the main factors that influenced the formation of beaded fibers, increased as the polymer concentration increased, the viscosity increased more rapidly and was the main factor influencing the character of electrospun nanofibers. In the dilute regime there are fewer polymer chain entanglements between macromolecules. The viscosity of a dilute polymer solution is therefore low, approaching the viscosity of the solvent and hence resulting in electrospraying. In a semi-dilute regime, polymer molecules act as separate coils, but crowding and touching each other. Interactions between polymer chains therefore increase, producing significant increases in viscosity. Electrospinning in the semi-dilute regime produces thinner nanofibers, which may be beaded [Huang (2006)]

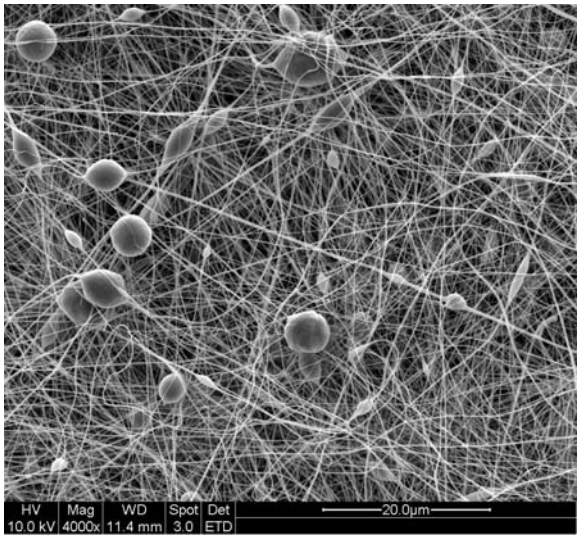

0.07 g/ml

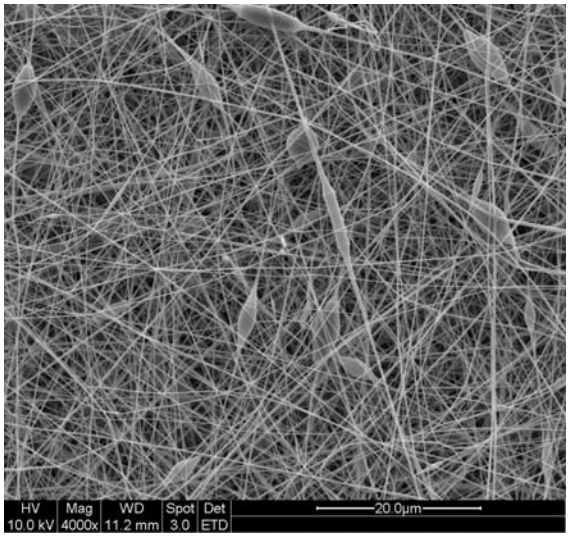

0.09 g/ml

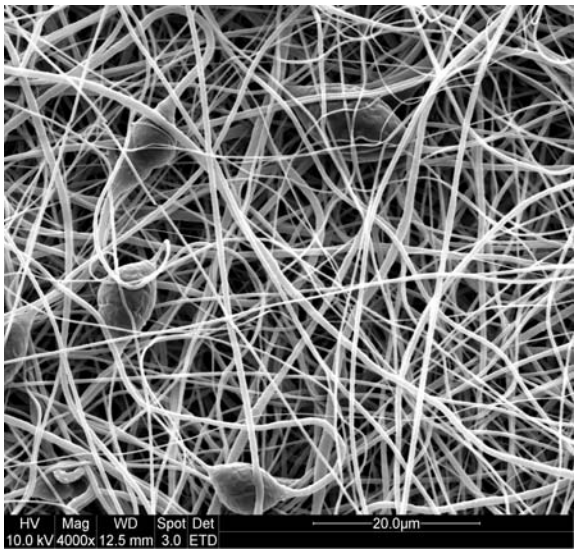

0.11 g/ml

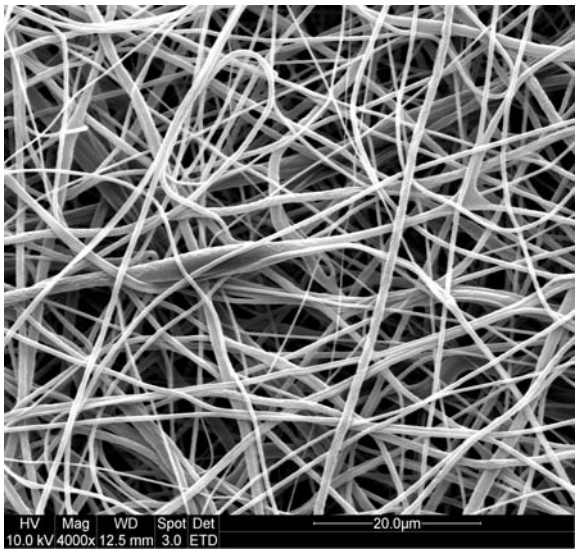

0.13 g/ml

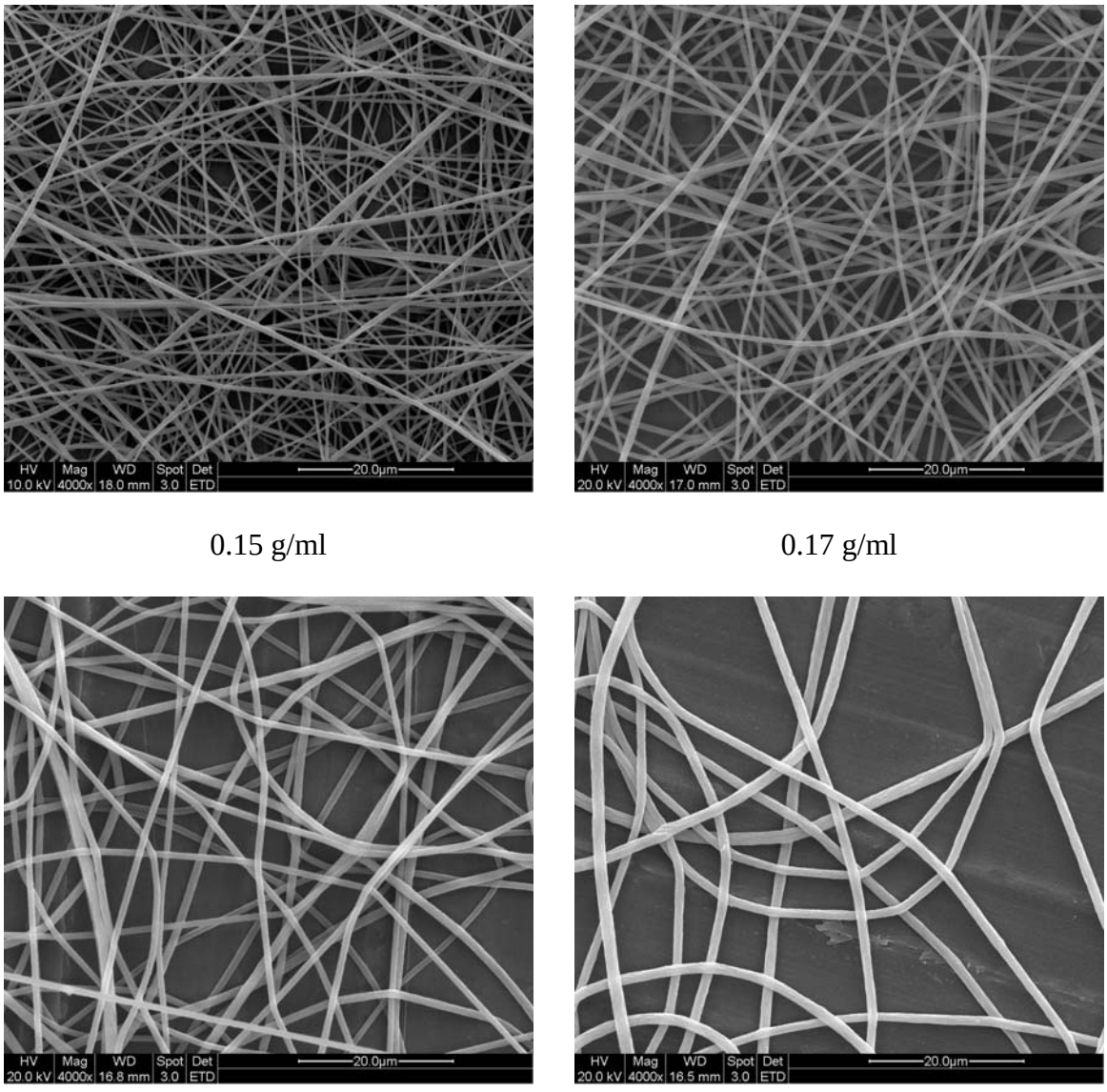

0.15 g/ml 0.17 g/ml

0.2 g/ml 0.25 g/ml

Figure 3.5: SEM micrographs of PVDF fibers electrospun at different concentrations

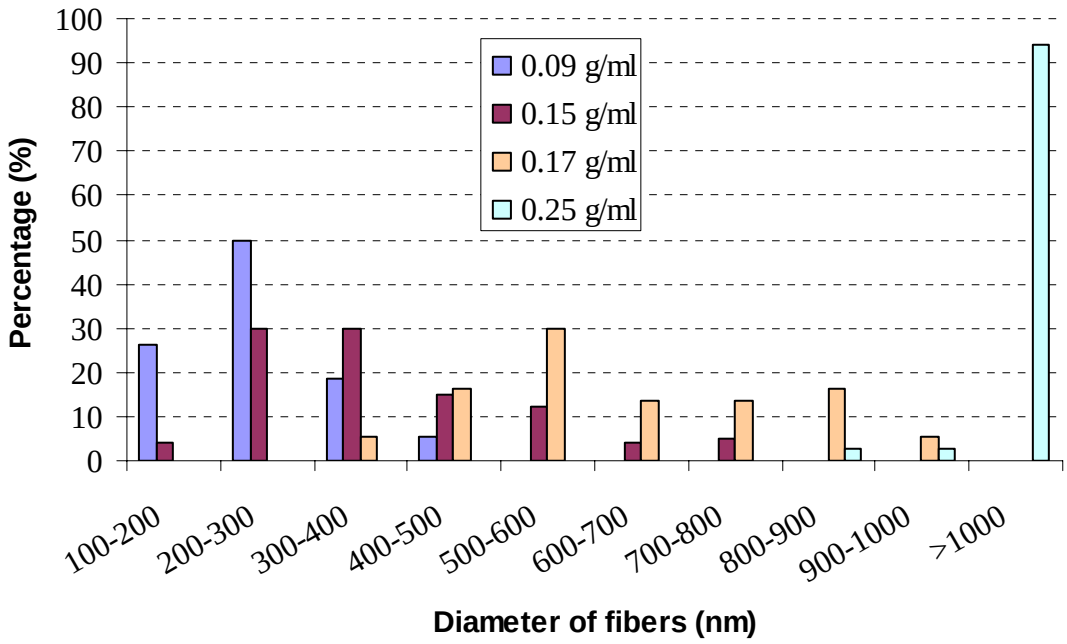

Figure 3.6: Fiber size distribution of PVDF electrospun at 0.09 g/ml, 0.15 g/ml, 0.17 g/ml and 0.25 g/ml

Another observation made was that as the concentration of the polymer solution increases, the fiber diameter increases. Some of the concentrations were selected and a fiber distribution profile was plotted and is expressed in Figure 3.6. At a concentration of 0.09 g/ml, the fiber size was generally less than 500 nm with an average of 249 ± 80 nm. As the concentration was raised to 0.15 g/ml, the largest fiber diameter was less than 800 nm with an average of 381 ± 147 nm. When the concentration was increased by 0.02 g/ml, the fiber distribution shifted to the right and the largest fiber size was less than 1000 nm and the average was calculated at 630 ± 163 nm which is almost 1.7 times that of the concentration of 0.15 g/ml. Finally when the concentration was raised to 0.25 g/ml, the fiber size increased tremendously and the smallest fiber lies in 800 nm to 900 nm region with an average diameter of

1341 ± 258 nm. As observed from Table 3.5, the average diameter and standard deviation increases with increasing concentration and a small change in concentration of 0.02 g/ml has a large influence on the fiber size.

Concentration (g/ml)	Average fiber diameter (nm) ± S.D.
0.09	249 ± 80
0.15	381 ± 147
0.17	630 ± 163
0.25	1341 ± 258

Table 3.5: Average fiber diameter of PVDF fibers electrospun at different concentrations

Since the concentration 0.15 g/ml has no beads and the smallest fiber size among the other concentrations which produced non-beaded fibers, this concentration was chosen to study the influence of feed rate on the fiber diameter.

3.2.2.5 Effect of Feed rate

The above experiments were conducted at 1 ml/hr feed rate. However in order to collect a membrane of thickness of approximate 120 μm, a total volume of 2.5 ml is required to fill up a 10 cm by 10 cm collector. Hence a waiting time of two and a half hours is required which is rather long. Hence the feed rate was increased to produce fibers at a faster speed. Feed rate of 2, 4, 8 and 16 ml/hr were carried out and the average fiber diameter and fiber diameter distribution is reflected in Table 3.6 and Figure 3.7. As can be seen from the mean fiber diameter, an increase in feed rate resulted in an increase in the average fiber diameter and a shift of the fiber

distribution towards the right. However there was no significance difference in the fiber diameter at a feed rate of 2 ml/hr and 4ml/hr. This might be because the feed rate was at the same rate at which the solution is carried away by the electrospinning jet with a corresponding increase in charges when the feed rate was increased. Thus there was a corresponding increase in the stretching of the solution which counters the increased diameter due to increased volume. However when the feed rate was increased to 8 and 16 ml/hr not only did the fiber diameter increase tremendously, but the overall membrane became very electrostatic and was subsequently difficult to handle. In addition to this, at a feed rate of 16 ml/hr some beads were observed (Figure 3.8). This is because there is a greater volume of solution being drawn from the needle tip and the jet produced is not stable and tends to break up.

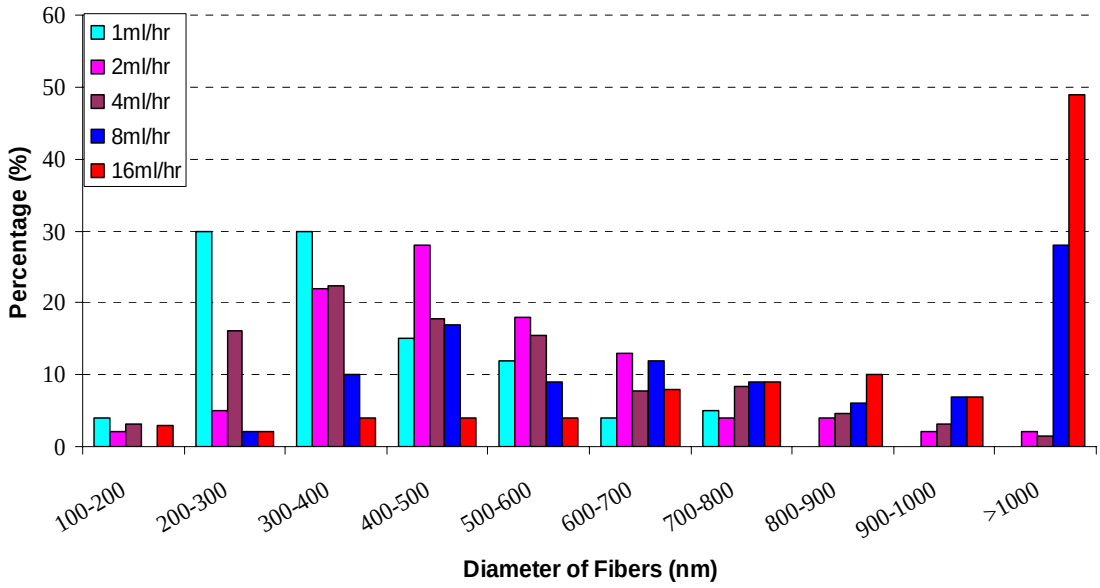

Figure 3.7: Size distribution of fibers produced at different feed rates of 1,2,4,8 and 16 ml/hr at a fixed concentration of 0.15 g/ml (DMAC:AC (40:60 v/v))

Rate	Average fiber diameter (nm) ± S.D.

1 ml/hr	381 ± 147
2 ml/hr	545 ± 247
4 ml/hr	490 ± 211
8 ml/hr	831 ± 466
16 ml/hr	1081 ± 539

Table 3.6: Average fiber diameter of PVDF fibers electrospun at different feed rates.

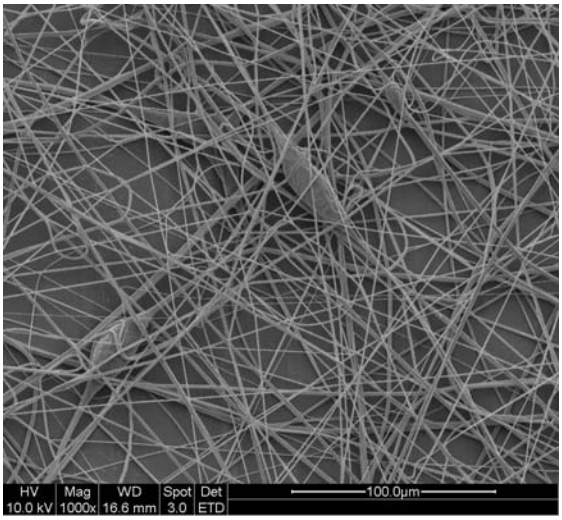

Figure 3.8: SEM picture of fibers produced at a feed rate of 16 ml/hr

By increasing the feed rate, the fiber diameter is compromised. Having too low a feed rate affects the productivity. As such the feed rate of 4ml/hr has been chosen to produce electrospun membrane which was subjected to further treatments.

3.3 Heat treatment of ENM

Electrospun PVDF membrane has a 'cotton like' texture and it is very difficult to peel from the aluminum plate without distorting the membrane. In the process of peeling, the fibers are stretched and some part of the membrane becomes thinner then the other, hence the membrane gets distorted. The as-spun membranes have very 'loose' strands of fibers on the surface that tend to come off easily. These 'loose' strands of fibers are also very electrostatic and hence making the overall membrane very difficult to handle. Hence it is desirable to fuse the fibers together so that a smooth and strong membrane can be obtained. This can be achieved by heat treatment.

The fibrous membrane was subjected to heat treatment to improve the mechanical strength of the fibers. PVDF has a melting temperature range of 134^0C to 169^0C. Hence heat treatment has to be applied below the melting temperature of the electrospun nanofiber membrane.

3.3.1 Methodology

The top surface of the electrospun membrane was covered with aluminum foil and then flattened with a roller and a plate weighing approximately 100g was placed on the surface of the membrane. When the temperature was raised to 150^0C, there were regions on the membrane that formed transparent film. This happened occasionally. This could have been due to the trapped solvents that were heated and dissolved some parts of the polymer. Hence as a precaution, the heavy plate was removed and only the aluminum foil was used to cover the top surface of the membrane. There were

times that the aluminum foil ballooned and this was again because of the trapped solvents trying to escape. Hence to maintain consistency, the electrospun membrane was initially heated at 60^0C for one hour to remove any trapped residual solvent. The temperature was then subsequently raised at 2^0C/min to a temperature below the melting temperature of the PVDF ENM and heated at that temperature for 3 hours and then cooled at a rate of 5^0C/min to room temperature. To determine the heat treatment temperature of the ENM, a differential scanning calorimeter (DSC) scan was performed on the PVDF ENM.

3.3.2 Thermal analysis

Differential scanning calorimeter (DSC) is a technique employed to determine the thermal transitions such as glass transition (Tg), melting temperature (Tm) or the crystallisation temperature (Tc) of a polymer. Only certain polymers exhibit a Tc. A profile of the thermal transitions can be observed in Figure 3.9.

The Tc and Tm is usually evident for polymers that can form crystals and a completely amorphous polymer do not have such transitions as they do not crystallize nor melt.

In this research work, only the Tm of the PVDF is required to determine the post heat treatment of the nanofiber membranes and the Tm profile can be used to explain any change of crystallinity of the polymer when the morphology of the substrate has changed. The degree of crystallinity can be obtained from the area under the peak

corresponding to melting per unit weight of polymer. This gives the enthalpy of fusion (J/g). To calculate the crystallinity, the enthalpy for the 100% crystalline material must be known.

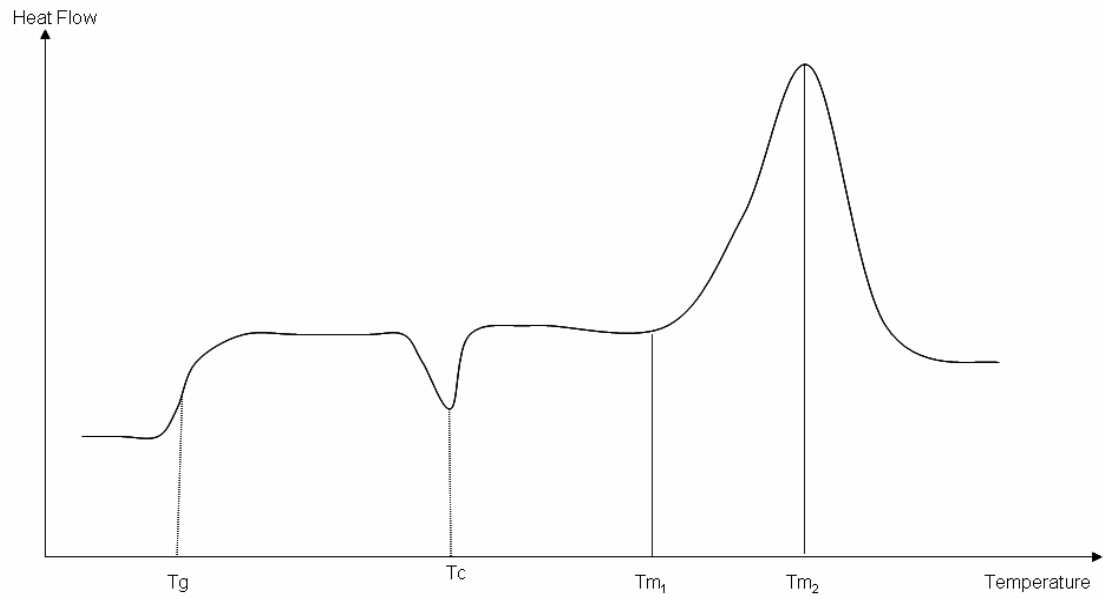

Figure 3.9: A typical DSC plot of a polymer

Thermal analysis of the PVDF pellet and electrospun membrane was performed on a differential scanning calorimeter (Perkin Elmer, Pyris 6) from a temperature range of 20^0C to 200^0C at a rate of 10^0C/minute. Table 3.7 shows the onset temperature, peak temperature of PVDF pellet and PVDF ENM.

Material	**Mass (g)**	**Onset Temp. (^{0}C)**	**Peak Temp. (^{0}C)**	**ΔH (J/g)**
PVDF pellet	5.3	161.2	170.0	33.59
Non heat treated ENM	5.4	158.2	167.1	51.67

Table 3.7: Thermal transitions of PVDF pellet and non heat treated ENM

The onset temperature was determined as 157^0C. Hence heat treatment was applied before this temperature. The membranes were placed in a vacuum oven to remove residual solvent before heat treatment was applied. Heat treatment was performed at 150^0C for 3 hrs. From the SEM micrographs in Figure 3.10 it was evident that overlapping fibers fused over one another. The heat treated ENM was sufficiently flexible to be folded without any distortion to the membrane and is easily stamped out into circular shape for water flux characterization at a later stage.

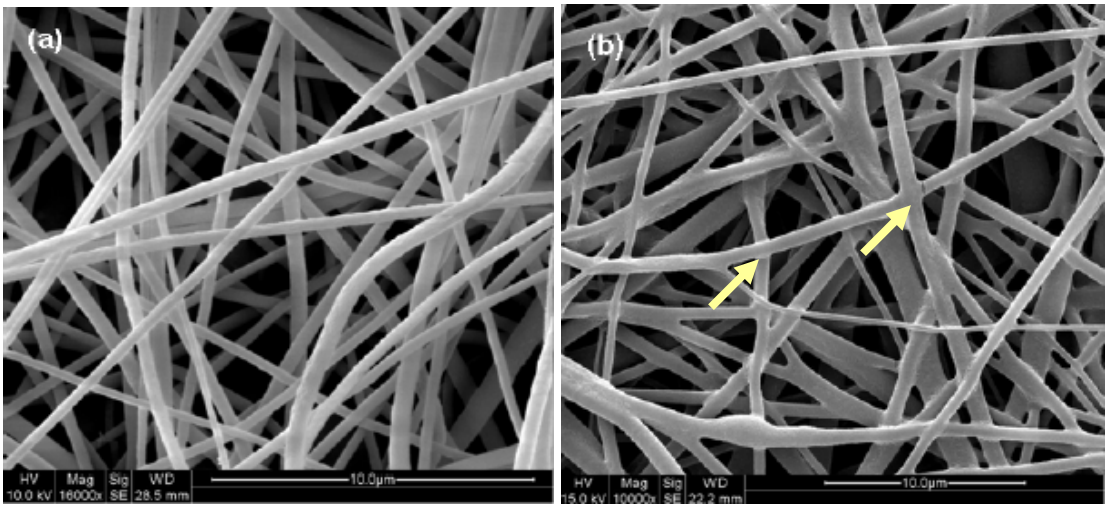

Figure 3.10: Electrospun PVDF EMN (a) before heat treatment, (b) after heat treatment. The arrows in (b) point out the fusion between the fibers.

The heat treated ENM (at 150^0C for three hours) was subjected to DSC analysis. Figure 3.11 reflects that the heat treated ENM possessed two melting peaks unlike the native ENM and PVDF pellet. A double endotherm in the melting region on a DSC scan is generally found in semi crystalline polymers. Two interpretations have been presented for this phenomenon. One is that the lower-temperature endotherm does not correspond to melting of a crystalline phase, but rather to a solid-solid phase

transition or partial melting, and that the higher temperature endotherm indicates melting of the crystalline phase formed by such transitions as orientations changes of crystals, phase transition between crystalline modifications or recrystalization. The other interpretation is that the two enotherms were attributable to the melting of two different crystalline phases initially coexisting. Generally solid phase PVDF can exhibit three different spherulitic crystalline forms: phase I, phase II and phase III, depending upon the method of production [Nakagawa (1973)]. The degree of crystallinity of PVDF normally ranges from 35-65% [Dohany (1980), Glennon (1997)]. The degree of crystallinity does not go beyond 65% due to two factors: the polymer is inherently easy to crystallize because of simple structure of its monomer but more complete crystallization is inhibited because of the presence of head to head structure in a polymer chain. The degree of crystallinity was calculated by the expression:

$$H_c = \frac{H_f}{H_f^0} \times 100\%$$

Where H_f is the heat of fusion for the tested sample and H_f^0 = 104.7 J/g [Nakagawa and Ishida (1973)], the heat of fusion for the 100% crystalline sample. Table 3.8 reflects the percentage crystallinity of PVDF pellet, non heat treated PVDF ENM and heat treated PVDF ENM. It is clear that PVDF in the pellet form has a low degree of crystallinity of 32% and when it was electrospun into fibers, the degree of crystallinity increased by 17%. However when the ENM was heat treated, the degree of crystallinity increased by almost twice. This highlights the presence of more

ordered structures within the fibers and the degree of orderness is increased further when the overall membrane was heat treated.

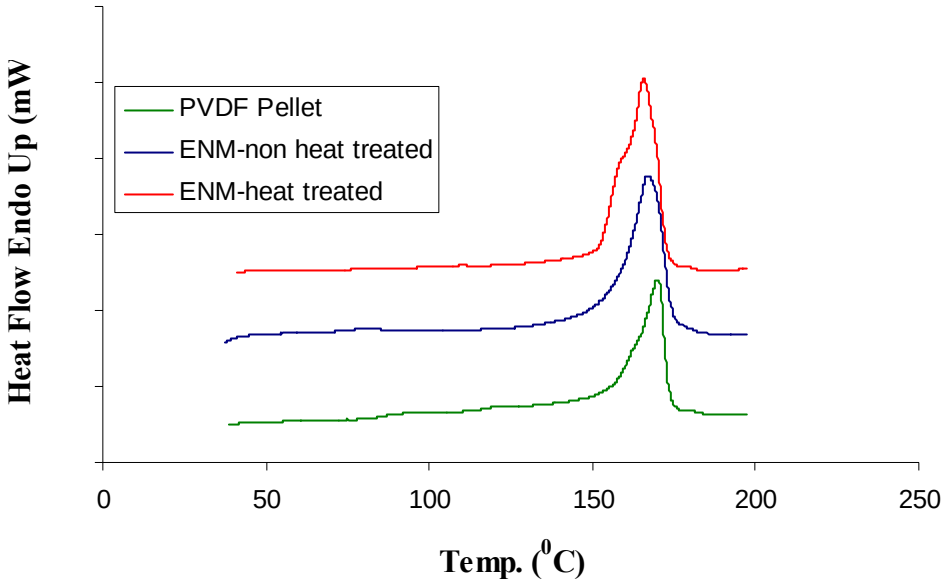

Figure 3.8: Melting transition of PVDF pellet, non-heat treated ENM and heat treated ENM

Material	Mass (g)	Onset Temp. (^{0}C)	Peak Temp. (^{0}C)	H_f(J/g)	Degree of Crystallinity H_c (%)
PVDF Pellet	5.3	161.2	170.0	33.59	32
Non heat treated ENM	5.4	158.2	167.1	51.67	49
Heat treated ENM	54	157.7	165.8	66.34	63

Table 3.8: Degree of crystallinity of PVDF in pellet and heat and non heat treated ENM form

3.3.3 Mechanical analysis

One draw back of the as-spun ENM was its poor mechanical strength. It had cotton like texture and thus could not function as a filter. To overcome this, the ENM was heat treated under 150^{0}C for 3h to improve the membrane's overall structural

integrity. The mechanical properties of the heat treated and non-heat treated ENM were tested in a tensile machine equipped with a 100N load cell. Three strips of length 3 cm by 1 cm were cut from each type of membrane. Tensile test was conducted using Instron 3345.

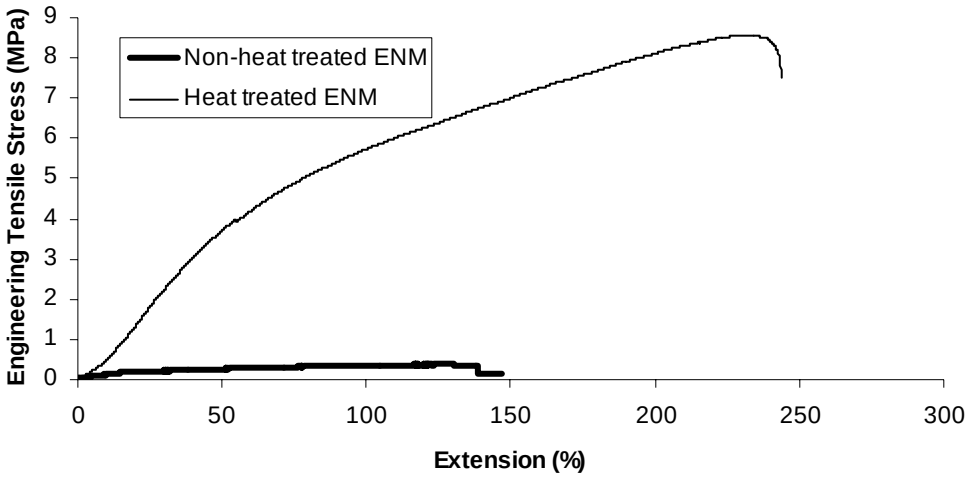

Figure 3.12: Mechanical strength of heat treated and non-heat treated ENM

The heat treated membrane became sufficiently rigid to be used for further characterizations. The increase in rigidity is evident from the tensile profile shown in Figure 3.12. The heat treated membrane had a significantly higher mechanical strength (8.5 MPa) compared to the non-heat treated ENM (0.4 MPa).

3.4 Conclusion

Factors such as MW, solvent, concentration and feed rate affect the fiber morphology of PVDF. The most suitable parameters to electrospin PVDF were when PVDF had a molecular weight of 440, 000 g/ml and dissolved at a concentration of 0.15 g/ml in a solvent combination of DMAC and AC (40:60 v/v) when subjected to a high voltage of 15 kV and a feed rate of 4 ml/hr at 70% humidity. This combination of parameters produced fibers with an average diameter of 490 ± 211nm. However the membrane generated after electrospinning was 'fluffy' and weak in structure. Post heat treatment at 150^0C for 3 hours improved the mechanical strength of the overall membrane. The electrospun membrane produced was utilized for the next series of experiments that is presented in Chapter 4 and Chapter 5.

Chapter 4

Surface Modification of Membranes

4.1 Plasma induced graft copolymerization of membranes

This section is geared towards the modification of the surface of ENM. Alongside to this, commercial hydrophobic PVDF membranes were modified and comparisons were made.

4.2 Methodology

Commercial hydrophobic PVDF membranes (HVHP, Millipore, USA) with a pore size of 0.45 microns and ENM membranes were cut into strips of dimension 1 cm by 2 cm and placed in a March Instruments Incorporated glow discharge plasma system. The plasma system is equipped with two parallel electrode plates and is fixed with a radio frequency power of 13.6 MHz. The glow discharge was produced at a plasma power of 30 W. Argon gas pressure was adjusted to 275 millitorr. The top surfaces of the membranes were exposed to plasma. The exposure to plasma was varied at 30, 60, 90 and 120 seconds. After plasma pretreatment, the membrane surface was exposed to air for approximately 10 mins to facilitate the formation of surface oxide and peroxide [Suzuki (1986), Clouet (1992)] before graft co-polymerization was carried out.

The membranes were subsequently placed in a glass tube containing aqueous solution of 10% (v/v) methacrylic acid (MAA) (Sigma-Aldrich, Germany) monomer and

sealed with a silicon rubber stopper. MAA was purified *in vacuo* to remove inhibitors that prevent polymerization. The tube was repeatedly vacuumed and purged with argon gas to remove dissolved oxygen. This set up is shown in Figure 4.1.

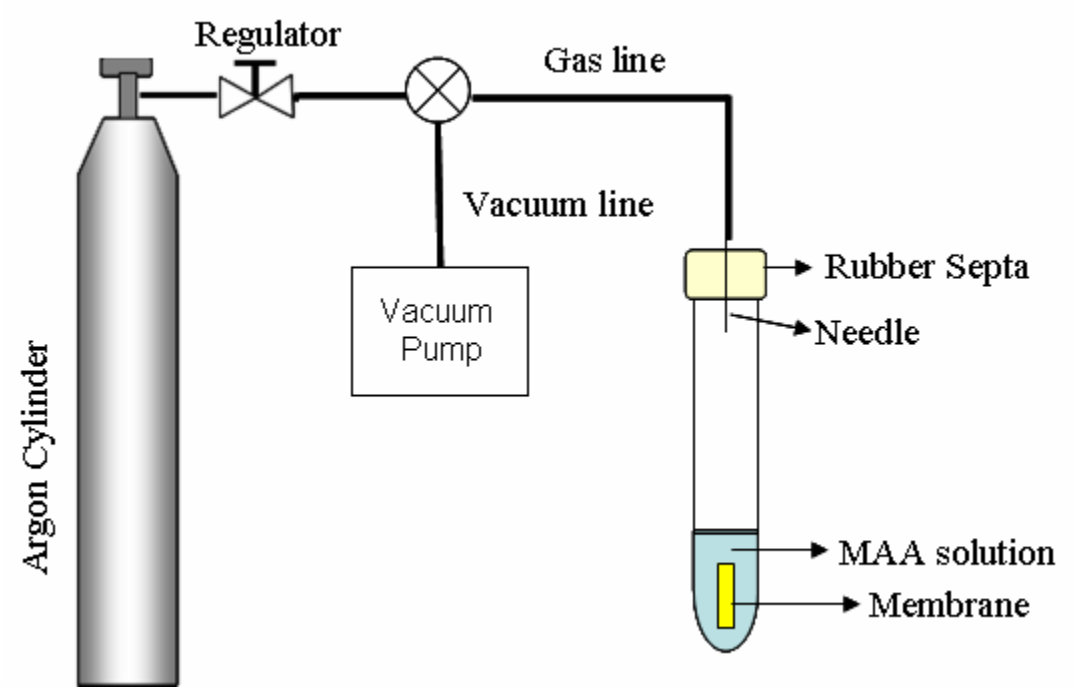

Figure 4.1: Illustrations of purging and vacuuming MAA solution containing the membrane to remove dissolved oxygen

Subsequently, the tube was heated at 80^0C for one hour to initiate graft co-polymerization. Copolymerization was terminated by removing the silicone stopper and exposing the tube to air. The PMAA-grafted membranes were washed with copious amount of deionized (DI) water followed by soaking in 0.1M NaOH (Merck, Germany) solution at 25.5^0C overnight under gentle shaking to remove physically adsorbed homopolymer and unreacted monomers. The schematic of this plasma induced graft polymerization is shown in Figure 4.2.

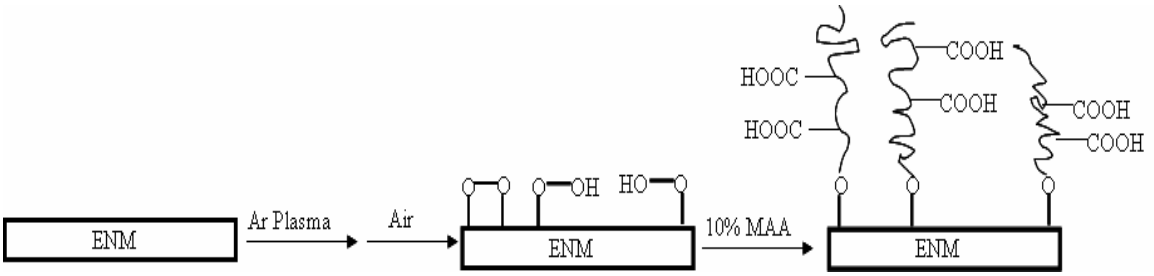

Figure 4.2: Schematic illustrations of surface modification process of the PVDF ENM

The grafting density of PMAA on the surface of ENM and HVHP were evaluated using Toluidine Blue (TBO) dye method [Uchida (1993), Ma (2006)]. The TBO dye specifically interacts with the carboxyl groups on the PMAA. The membranes were placed in a TBO (Aldrich, Germany) solution (30mg of TBO dissolved in 200ml of 0.1M NaOH) for 3 hours followed by thorough rinsing with NaOH solution (pH=10) to remove any unbound TBO molecules. The stained membranes were then dried before immersing them into 50% acetic acid (BDH, England) which unbinds the TBO from the carboxyl groups of the PMMA. The absorbance of the solution at 620 nm was measured using a UV-Vis spectrophotomer (Unicam UV 300, Thermo Spectronic). The amount of carboxyl groups on the PMMA is directly proportional to the adsorbed TBO amount. A calibration curve of different concentration of TBO against its respective absorbance value was plotted and with reference to this curve, the grafting density at different plasma pretreatment time was determined.

The change in the surface chemistry of the non-grafted ENM and HVHP and the surface modified ENM and HVHP were detected using a single bounce horizontal

ATR-FTIR (Thermo Nicolet Avatar 360, USA). The ATR accessory (Avatar^{TM} OMINI-Sampler^{TM} accessory) contained a Germanium crystal at a nominal incident angle at 45^0. Each spectrum was obtained by accumulating 64 scans at a resolution of 4 cm^{-1}.

Scanning electron microscope (SEM) (Quanta 200F, FEI, Netherlands) was used to observe the change in surface morphology of the non-grafted and grafted membranes. The membranes were sputtered with a thin layer of gold before being placed in the SEM chamber. Coated samples were examined at an accelerating voltage of 10 kV.

Static water contact angle (WCA) measurements were performed on membranes using an Advanced Surface Technologies, Inc., VCA2000 (USA) video contact angle system. A water drop of 0.5 μL was dispersed on the membrane surface and the contact angle determined using the system software. The change in static contact angle with respect to time was measured.

4.3 Influence of exposure time on grafting density

The grafted surfaces of both ENM and HVHP turned orange and hence can be discriminated easily from the non-grafted surfaces. The function of plasma is to generate radicals on the surface of the membranes. The generation of free radicals can happen either through the bombardment of the ions and photons which can provide energy higher than the C-C or C-H bond hence breaking the respective bonds or through elastic or inelastic collision of the electron in the plasma with the polymer

resulting in the abstraction of a proton. In inert gas plasmas, the dominant process is hydrogen abstraction [Clouet (1992)].

When the membranes were exposed to air, these radicals react with the oxygen in the air to form peroxides. When immersed in a degassed MAA solution at 80^0C, these peroxides cleave to form radicals again and the radicals on the surface of the membranes react with the double bond of the MAA as double bonds are effective scavengers of radicals. More MAA monomers add on to the chain until the reaction is terminated with oxygen. The reaction mechanism is illustrated in Figure 4.3.

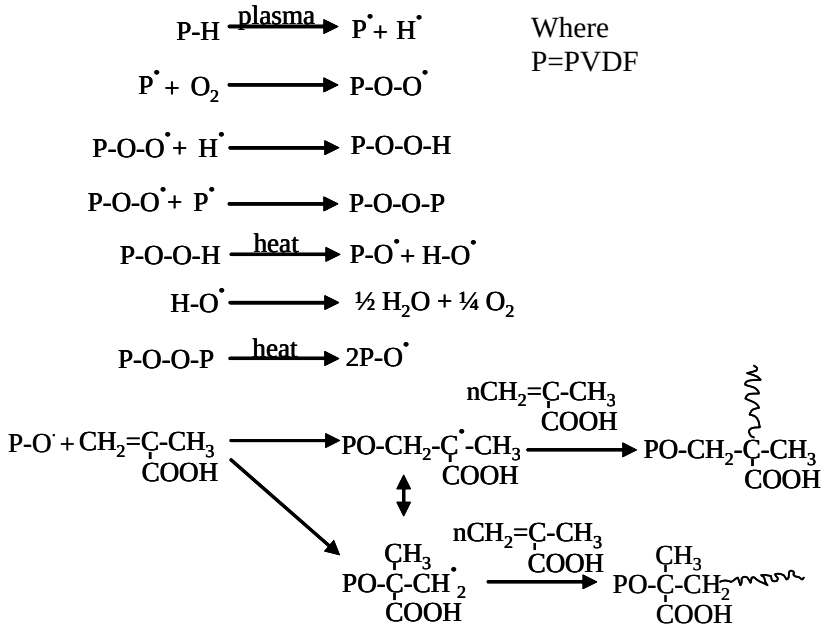

Figure 4.3: Reaction mechanism for plasma induced surface modification of PVDF ENM

Figure 4.4 shows the change in grafting density with respect to plasma exposure time for both the ENM and HVHP. At 30 sec of plasma exposure time followed by

grafting, HVHP had the same level of grafting density as ENM. Interestingly, beyond 30 sec the response of the membranes to plasma exposure time greatly varied. The rate of change of grafting density with exposure time for the ENM is significantly larger than that of HVHP. For the ENM, the graft density increased in a linear manner from 30s (23 nmol/mg) to 90s (170 nmol/mg) and gradually from 90s to 120s (180 nmol/mg). On the contrary, HVHP showed an increase in graft density from 30s (25 nmol/mg) to 60s (65 nmol/mg) and no significant change in graft density was observed with further increasing plasma exposure time.

As explained by Ikada et al. [Suzuki (1986)], the peroxide formation after plasma pretreatment facilitates grafting and the dependence of the peroxide formation on the glow discharge time is not monotonous but shows a maximum. The formation of peroxide group is directly related to the grafting density. Hence a longer exposure time does not necessarily generate higher amounts of peroxides. This was clearly observed for HVHP, where no significant change in graft density was observed beyond 60s. In the case of the ENM, there was a continuous linear increase in graft density up to 90s. From 90 to 120s there was an increase in the density but this was rather gradual. One possible reason for the significant difference in graft density between ENM and HVHP is the surface area of the membranes. ENMs by virtue of their small fibers possess high surface area and hence a larger area for grafting to occur. HVHP, on the other hand, has a much lower surface area. These differences in surface area will inevitably affect the grafting density.

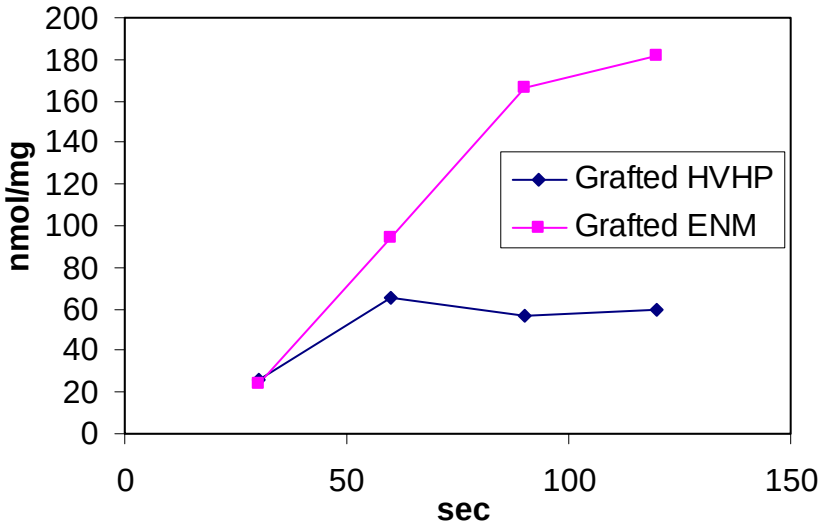

Figure 4.4: Grafting density of PMAA on the surface of ENM and HVHP

4.4 Influence of grafting on membrane surface morphology and chemistry

The effect of plasma induced graft co-polymerization on the morphology of the membranes was investigated with SEM. Figure 4.5a and 4.5b shows the surface topography of the ENM before and after grafting respectively. The ENM exhibits a fibrous and porous architecture and after grafting the fibers have grown 'thicker' and the pore size has reduced. It is to be noted that the morphology of the ENMs may look completely different when in water. Figure 4.6 gives a schematic illustration of how the PMAA chains may behave in the presence and absence of water. Figure 4.5c and Figure 4.5d represent the micrographs of prisitine HVHP and grafted HVHP correspondingly. According to the SEM micrographs, the pores of the grafted HVHP have been reduced more significantly than the ENM despite a lower grafting density. Grafting could have occurred within the ENM.

Figure 4.7 presents the typical ATR-FTIR spectra of the grafted and non grafted ENM. It is evident that the grafted ENM had additional peaks at ~3400 cm^{-1} and ~1600 cm^{-1} which respectively correspond to a hydroxyl and a carbonyl stretch of the carboxyl groups present in PMAA and these peaks are not observed for PVDF. Similarly, these additional peaks are present for the grafted HVHP and the spectrum is reflected in Figure 4.8.

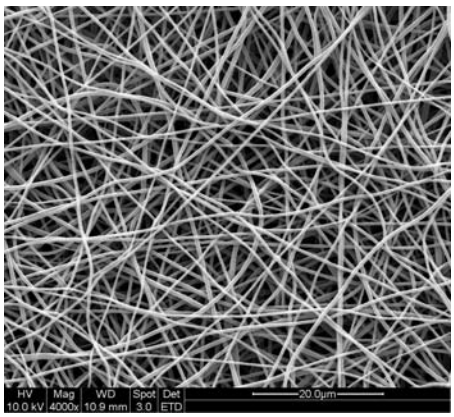

(a)

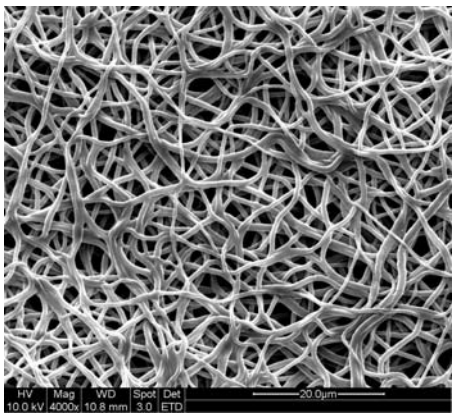

(b)

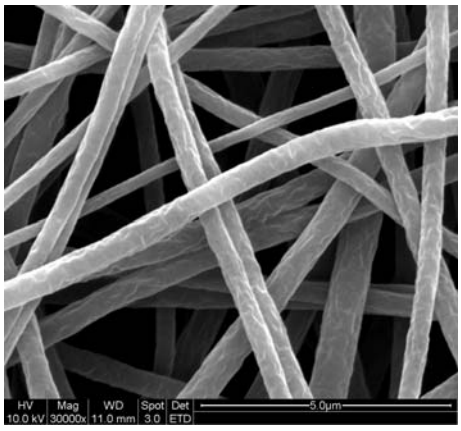

(c)

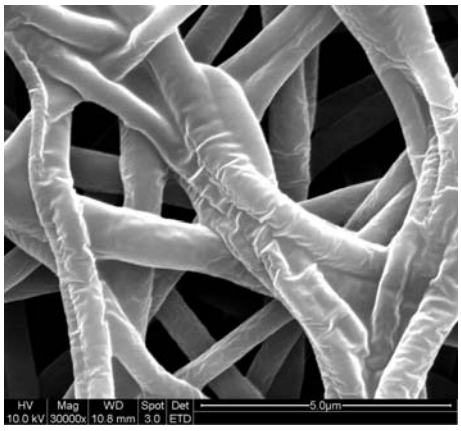

(d)

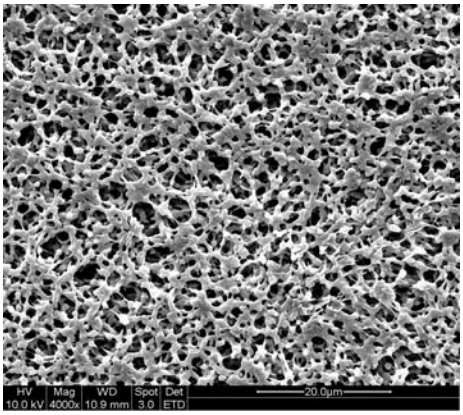

(e)

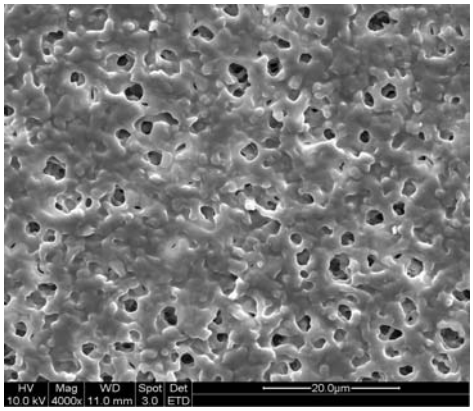

(f)

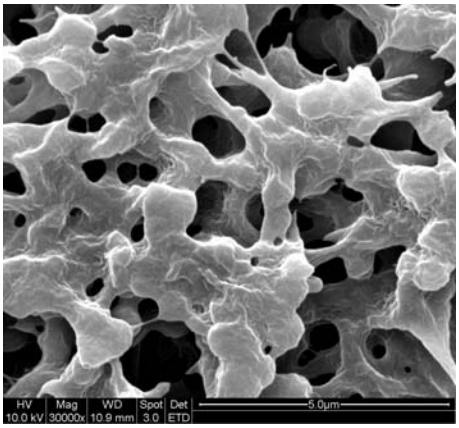

(g)

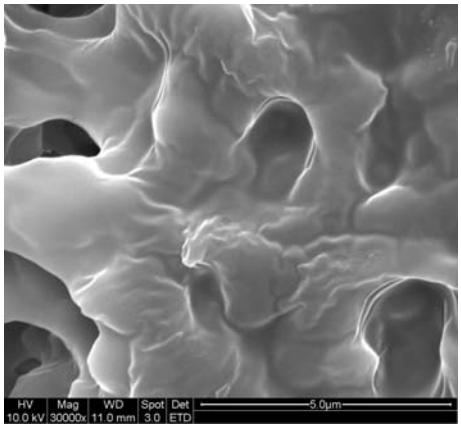

(h)

Figure 4.5: SEM Micrographs of (a) untreated NF (x 4000), (b) plasma treated NF after 90 sec (x 4000), (c) untreated NF at (x 30000), (d) plasma treated NF after 90 sec (x 30000), (e) untreated commercial membrane (x4000), (f) plasma treated commercial membrane after 90 sec (x 4000), (g) untreated commercial membrane (x 30000), (h) plasma treated commercial membrane after 90 sec (x 30000)

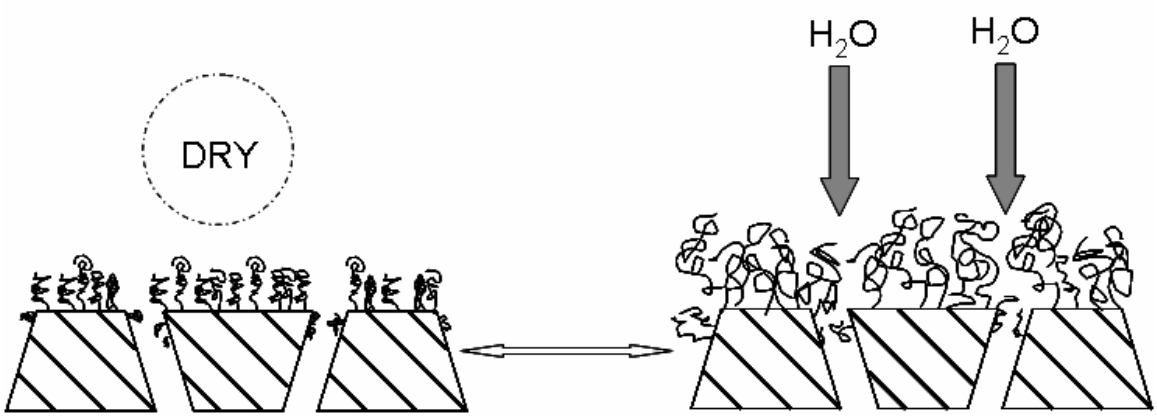

Figure. 4.6: Schematic diagram of how PMMA chains behave without and with water.

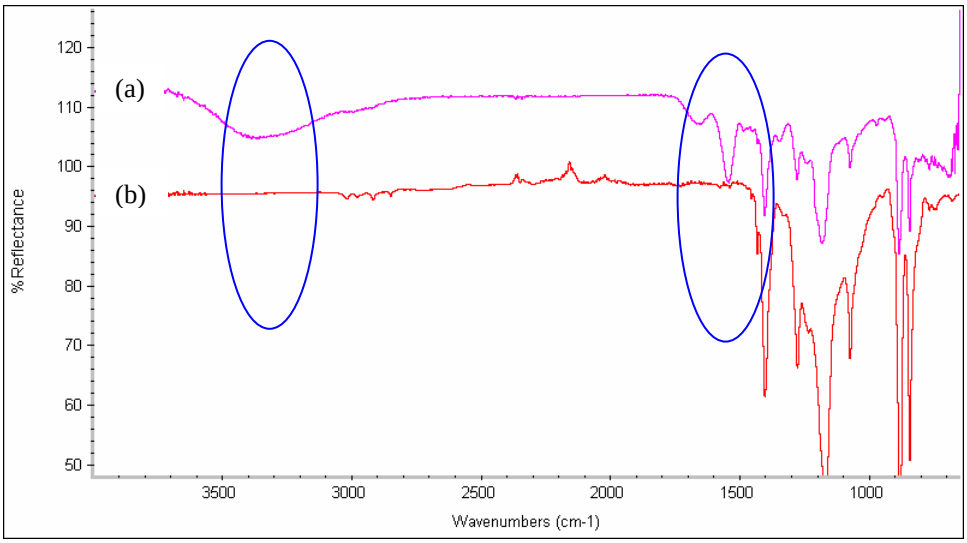

Figure 4.7: ATR-FTIR spectrum of (a) PMAA grafted ENM, (b) Pristine ENM. Additional peaks were observed for (a) and are circled.

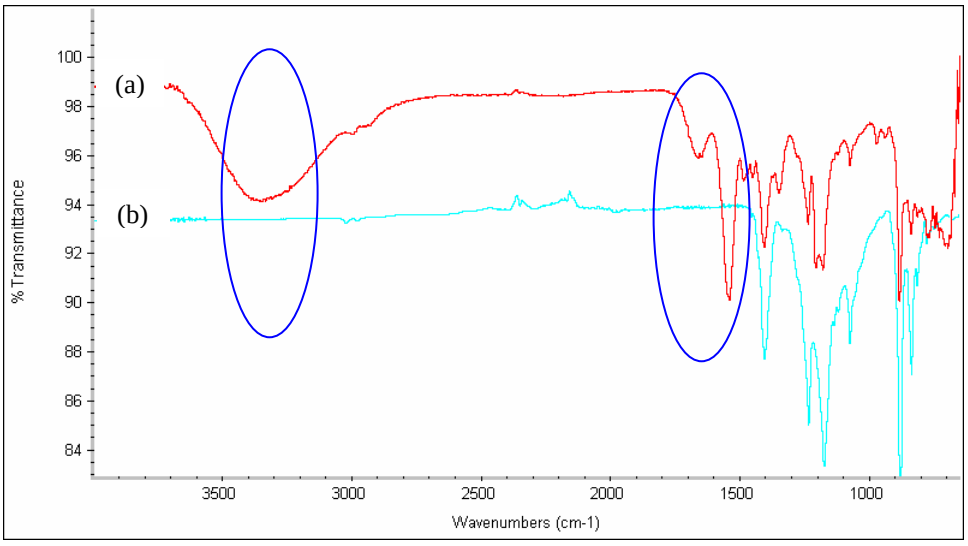

Figure 4.8: ATR-FTIR spectrum of (a) PMAA grafted commercial membrane, (b) Pristine commercial membrane. Additional peaks were observed for (a) and are circled.

The water contact angle of the non-grafted ENM was measured as 132.2 ± 9.1^0 and that of the HVHP was 124.2 ± 8.3^0. The increased hydrophobicity for the ENM is due to inherent surface roughness and trapped air pockets. However after grafting, the contact angle of the grafted ENM decreased rapidly with time and reached zero in a few seconds while for the grafted HVHP contact angle decrease was not as swift as the grafted ENM (see Figure 4.9). The difference between these two grafted membranes seems attributable to the difference in their morphology. As mentioned earlier, grafting could take place within the ENM due to its large pore size. If it happens, water can be drawn into the pore much faster than the grafted HVHP, where the grafting does not go deep inside the pore. As a result, the contact angle of the ENM decreases faster than the grafted HVHP

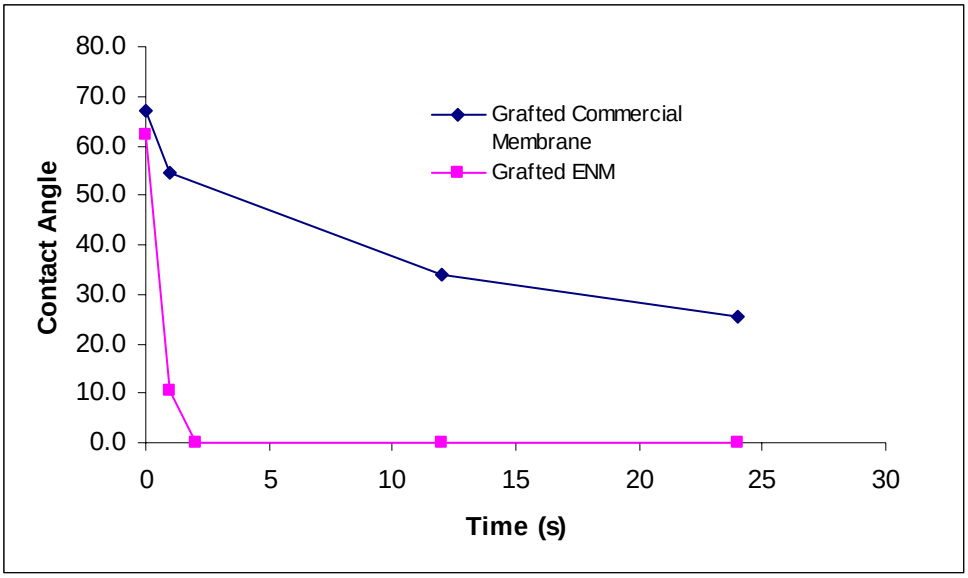

Figure 4.9: Water Contact angle of grafted ENM and HVHP

The water cannot penetrate inside a dry membrane unless a transmembrane hydrostatic pressure that exceeds the Liquid Entry Pressure of water (LEPw) is applied. It was anticipated that having a higher contact angle, ENM would exhibit a higher LEPw than HVHP. However, on the contrary, the LEPw of virgin ENM and HVHP were 5 psi and 14 psi respectively. This indicates that the increased hydrophobicity of ENMs is not a true indication of their resistance to wetting. The ENM possess very large surface pores compared to HVHP, thus a lower amount of pressure is required to overcome the initial surface resistance and allow water to pass through the membrane.

After grafting the LEPw of the ENM dropped to 0 psi, corresponding to the rapid decrease in the water contact angle within 2 seconds. The LEPw of the grafted HVHP membrane was higher at 3 psi. Although a hydrophilic group was grafted on the

surface of the commercial membrane, the pore size played a more dominant factor in determining the LEPw than the surface hydrophilicty. For the ENM, as the pores are generally much larger, the presence of hydrophilic groups had a more significant impact on the LEPw.

4.5 Conclusion

The surface of ENM has been successfully grafted with PMAA. The grafting density of ENM was more than HVHP because of the surface architecture of ENM which had a much larger surface area. The surface grafted ENMs exposed to argon plasma for 90s followed by subsequent grafting with PMAA at 80^0C for one hour would be used for the next set of experiments presented in Chapter 5.

Chapter 5

Membrane Characterization

5.1 Introduction

As mentioned in the literature review, there are two key factors that govern the efficiency of a membrane and they are flux and selectivity. A membrane that can produce a high selectivity and flux are desired. Characterization of a membrane in terms of porosity, pore-size, pore-size distribution, wettability (hydrophilic/hydrophobic), membrane thickness, flux permeability and separation selectivity will determine the type of separation processes and performance of a membrane.

This section will be geared to answer the following questions: Are ENMs capable of generating high flux? Will different morphology of ENMs, such as ENMs comprising of only fibers or fibers and beads or surface modified ENMs, affect the flux? How different is the water permeation characteristics of a surface modified ENM when compared to a commercial membrane with similar pore-size distribution?

5.2 Bubble point, mean flow pore and pore size distribution

The pore size distribution, bubble point and mean flow pore of several membranes listed in Table 5.1 were determined using a capillary flow porometer (Porous Materials Inc, USA) which is able to detect pore size from 0.013 to 500 microns.

The membranes were completely wetted with Galwick™ (Porous Materials Inc, USA) and pressure was applied on one side. As the gas pressure increase gradually, there will be no gas flow through the pores until capillary forces are overcome releasing liquid from the pore. The first gas bubble will emerge from the largest pore where the capillary forces are lowest. The pressure at which this occurs is called the "bubble point" pressure. The relationship between the pore-size and the corresponding pressure is given by the Young-Laplace equation:

$$R = \frac{2\gamma}{\Delta P}\cos\theta$$

where R is the radius of the pore, ΔP is the differential gas pressure, γ is the surface tension of the wetting liquid, Galwick™ (γ =15.9 dynes/cm) and θ is the wetting angle. The pressure is increased continuously until the liquid is displaced from the smallest pore and there is complete flow of gas through the membrane which equals that through a dry membrane. A pore size distribution is then calculated from these data. The mean pore size is then calculated by constructing a line equal to one half of the dry air flow through the membrane. The pressure at which the wet airflow intersects this line is the point at which the liquid has been expelled from one half of the pores [Mark (1990)].

Type of membrane	Abbreviation	Source of membrane
PVDF ENM with beads. Electrospun at 0.09 g/ml (DMAC:AC (40:60 v/v)), 1ml/hr. Diameter of fibers = 249 ± 80 nm	Beaded ENM (A)	Electrospun in the laboratory
PVDF ENM with beads. Electrospun at 0.15g/ml (DMAC:AC (70:30)), 4ml/hr Diameter of fibers = 472 ± 259 nm	Beaded ENM (B)	Electrospun in the laboratory
As-spun PVDF ENM without beads. Electrospun at 0.15 g/ml (DMAC:AC (40:60)), 4ml/hr. Diameter of fibers = 490 ± 211 nm	As-spun ENM	Electrospun in the laboratory
Surface modified as-spun PVDF ENM	Grafted ENM	Electrospun and surface modified in the laboratory
Commercially available hyrophobic PVDF	HVHP	Millipore, USA
Commercially available hydrophilic surface modified PVDF	HVLP	Millipore, USA

Table 5.1: Types of membranes and their source of purchase and abbreviation

5.2.1 Effect of Morphology

The effect of morphology on the pore size distribution was evaluated. It can be observed from Figure 5.1, Figure 5.2 and Table 5.2 that the bubble point for Beaded ENM (A) was much lower. This can be explained by two factors: (i) when the fibers are thin, they are closely packed and hence reduce the interconnected pore size; or (ii) the presence of beads blocked the pores. To confirm which factor is true, another system was electrospun where the fiber size was close to the as spun ENM but consist of beads. The pore size distribution of this membrane is reflected in Figure 5.3.

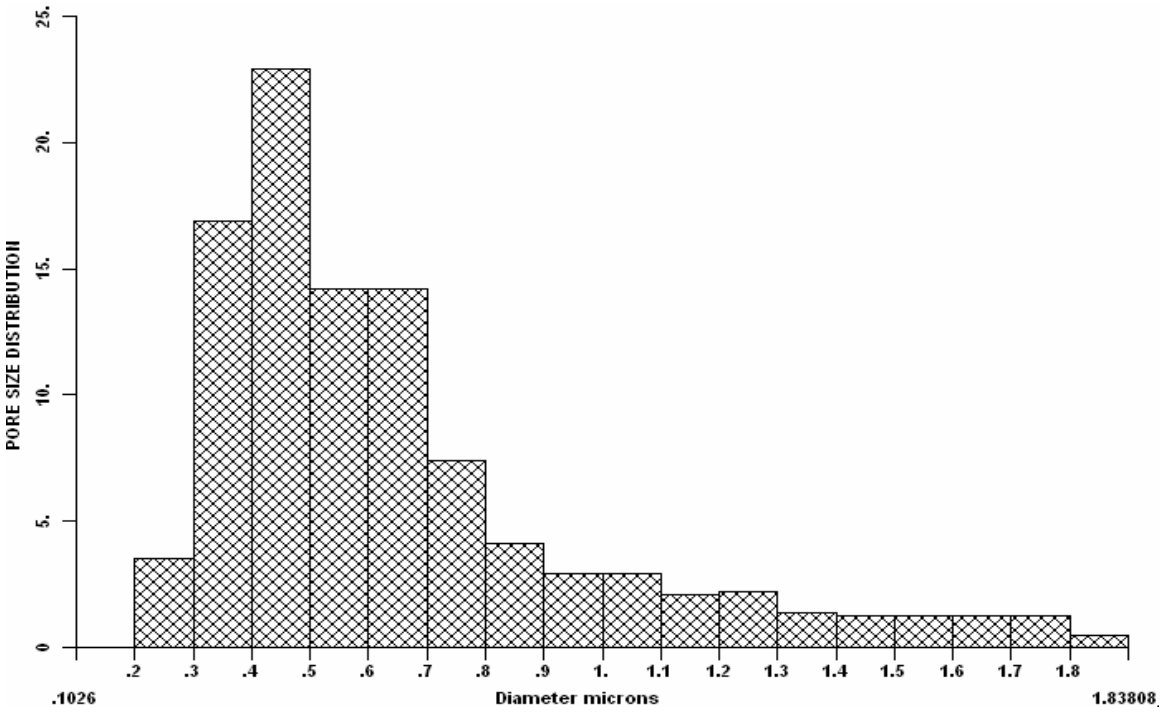

Figure 5.1: Pore size distribution of Beaded ENM (A)

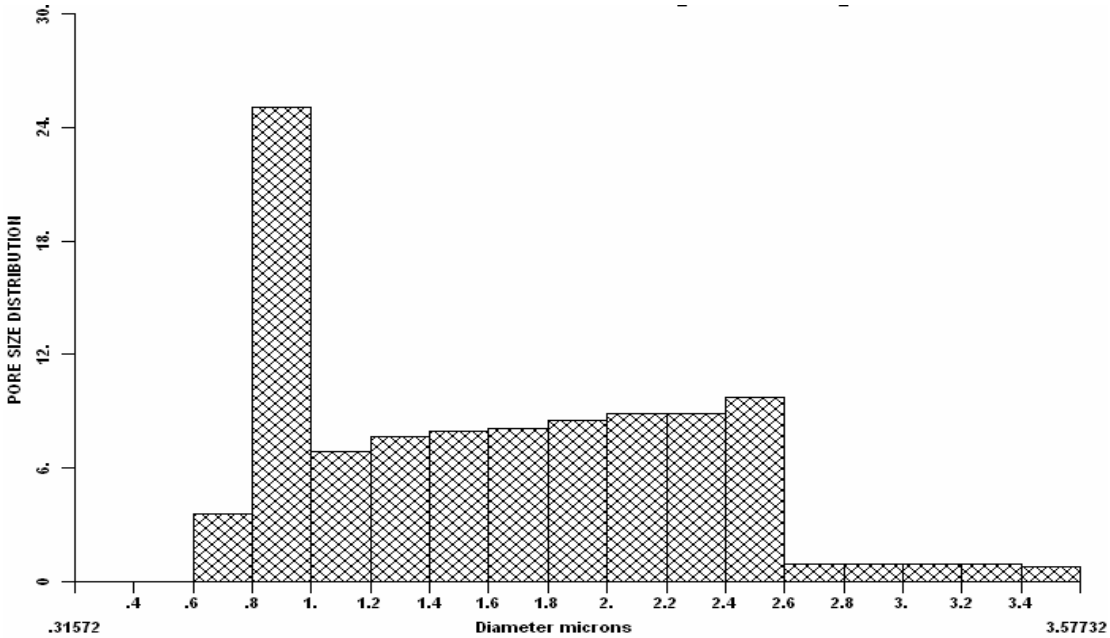

Figure 5.2: Pore size distribution of as-spun ENM

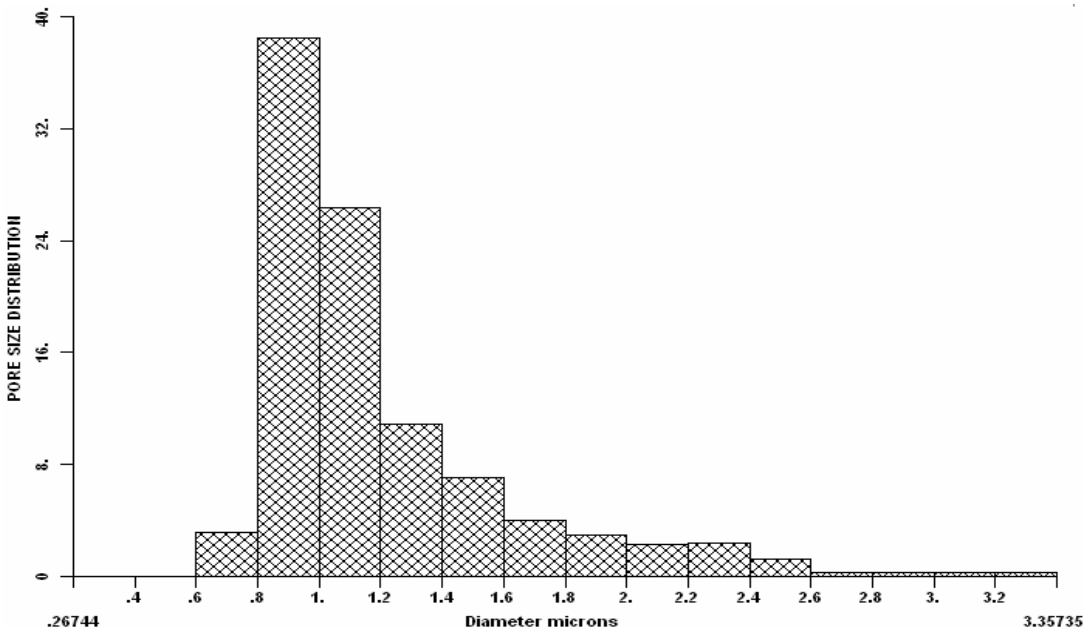

Figure 5.3: Pore size distribution of Beaded ENM (B)

Type of membrane	Bubble point diameter (μm)	Smallest pore (μm)	Highest frequency (μm)	Mean flow (μm)
Beaded ENM A	1.84	0.24	0.4 to 0.5	0.55
Beaded ENM B	3.36	0.80	0.8 to 0.1	1.03
As-spun ENM	3.58	0.72	0.8 to 0.1	1.58

Table 5.2: Pore-size distribution, highest frequency and mean flow diameters of ENMs with different morphologies

Figure 5.3 and Table 5.2 shows that the bubble point of the Beaded ENM (B) was very close to the as-spun ENM. Hence the presence of beads did not affect the bubble point and pore-size distribution but rather it is the fiber size that affects the packing distribution of the fibers and hence decreasing the pore size of the interconnected fibers.

5.2.2 Comparison of grafted-ENM and HVLP

Prior to grafting, the bubble point of the ENM was 3.58 μm and that of the HVHP was 0.91 μm. The smallest pore detected for the ENM was 0.72 μm while that of the HVHP is 0.22 μm. The pore size distributions of HVHP and as-spun ENM are presented in Figure 5.4 and Figure 5.2 respectively. From these data, it is obvious that ENM would have a different separation capability than a commercial membrane due to a large difference in their pore size distribution.

After grafting HVHP, its bubble point and its smallest pore was very much reduced and was beyond our equipment's capability to detect the smallest pore present. Hence

a comparison of the pore size distribution of the grafted ENM and a hydrophilic commercial 0.45 μm PVDF (HVLP) membrane was made instead. The largest pore (bubble point) of the grafted ENM was detected as 0.88 μm and that of the HVLP was 1 μm. However the pore-size distribution at the bubble point for both membranes was very low and hence reflected as zero in comparison to the other pore sizes. For the grafted ENM a distinguished pore size distribution is observed at 0.45 μm and below and comparatively for the HVLP it is at 0.5 μm and below. For both the membranes, the smallest pore size was 0.05 μm and the mode pore size was between 0.3 and 0.35 μm. The pore size distribution of the grafted ENM and HVHLP is presented in Figure 5.5 and Figure 5.6. The results indicate that it is possible to reduce the pore size of the ENM through surface grafting to achieve smaller pores. By optimizing the grafting conditions, it might be even possible to achieve pores in the range of ultrafiltration membranes.

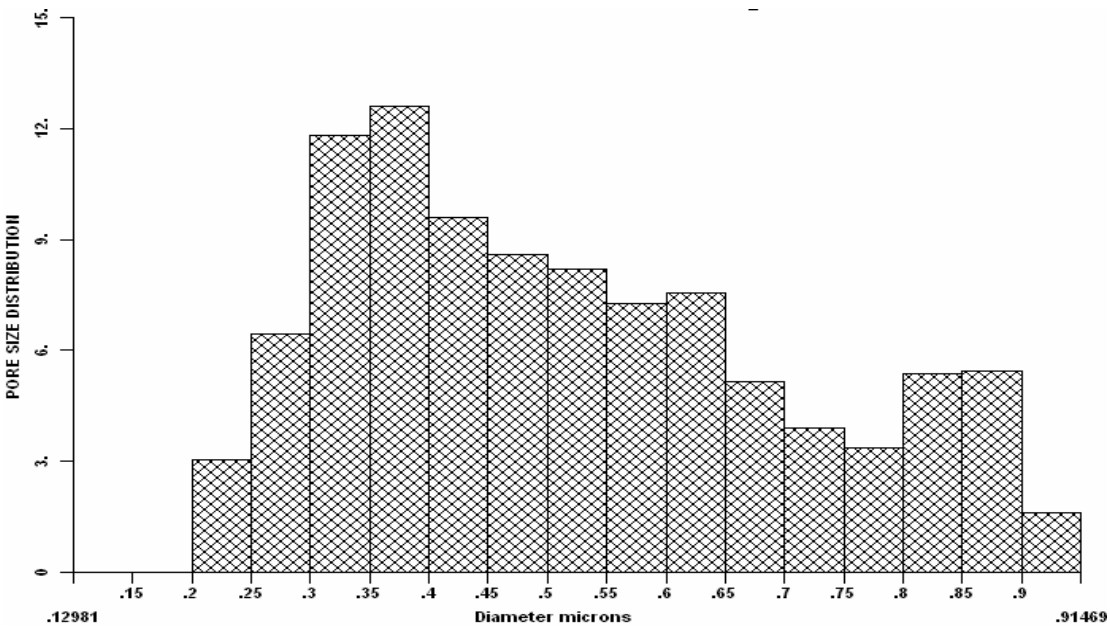

Figure 5.4: Pore size distribution of HVHP

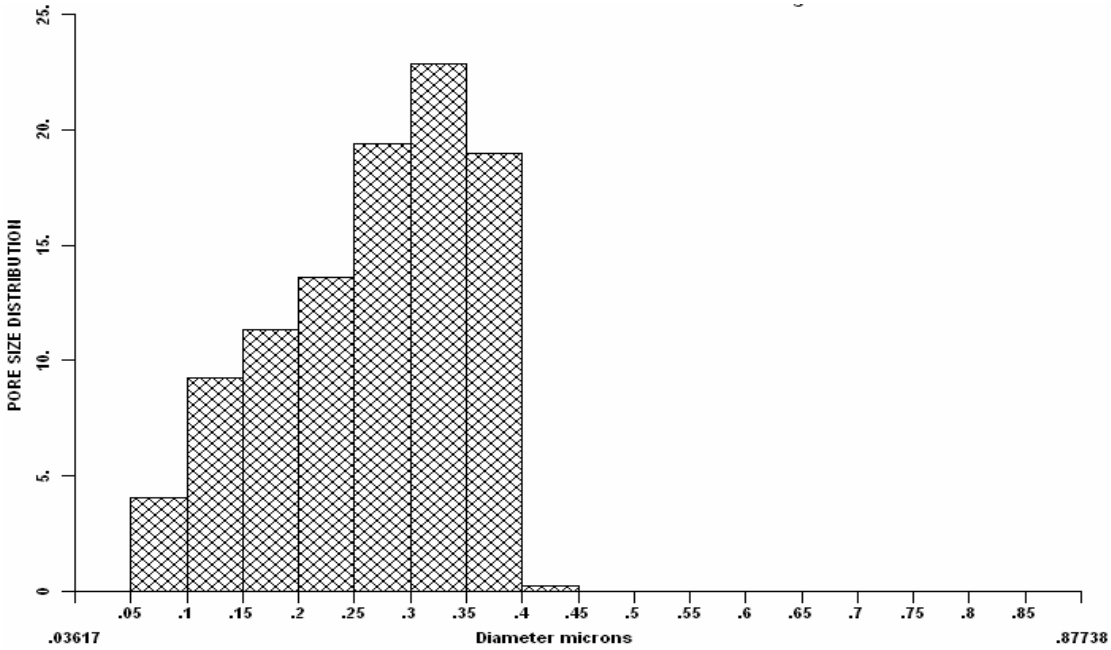

Figure 5.5: Pore size distribution of grafted ENM

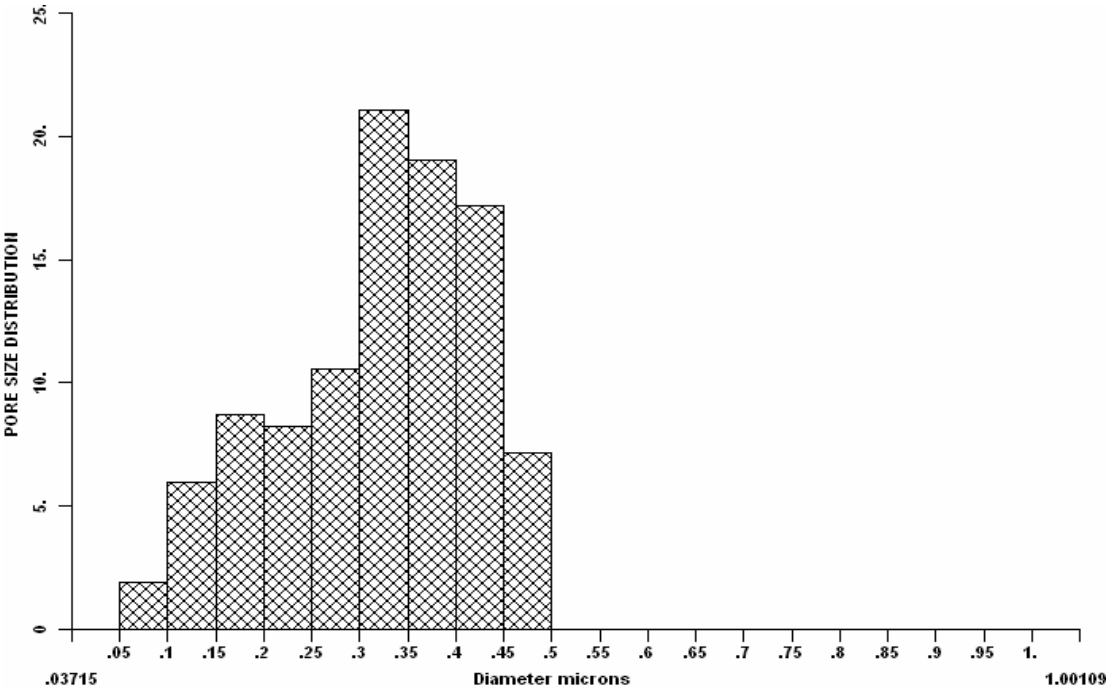

Figure 5.6: Pore size distribution of HVLP

5.3 Water flux permeation

Non-grafted ENM, grafted ENM, HVHP and HVLP, were used to determine the membrane performance using a simple dead end filtration cell set up as shown in Figure 5.7. The effective membrane diameter for all the membranes was kept constant at 1 cm. Dried membrane was placed in the membrane cell and filled with 350cm^3 of deionised (DI) water. The pressure was gradually increased and the pressure at which the first water droplet was observed at the permeate end was determined. This is defined as the liquid entry pressure of water (LEPw). The membrane was then removed from the cell, wetted with 50% ethanol and then immersed in DI water for 30 min to ensure the membranes were completely wet. The wetted membrane was then placed back in the cell for water flux study. The applied pressure was increased gradually and the corresponding water flux measured.

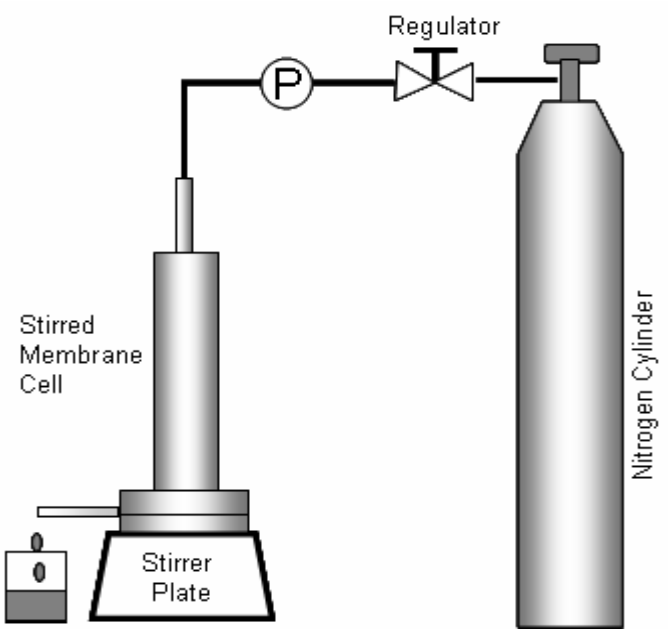

(a)

(b)

Figure 5.7: (a) Schematic illustrations of the water permeation set up and (b) the real set up used in the lab

5.3.1 Comparison of water flux performance of Beaded ENM (A) and as-spun ENM

As can be seen from Figure 5.8, the as-spun ENM had a much higher flux compared to Beaded ENM (A). This is attributed to the larger pores and porosity of the as-spun ENM. Hence selecting Beaded ENM (A) and grafting the top surface will not be appropriate if a high flux is desired. The base membrane should have significantly large pores and porosity to achieve high flux. If separation of smaller particle size is desired than this high flux base membrane can be surface modified where the modified surface is the separating layer and the porous base acts as a support and aids in achieving a high flux.

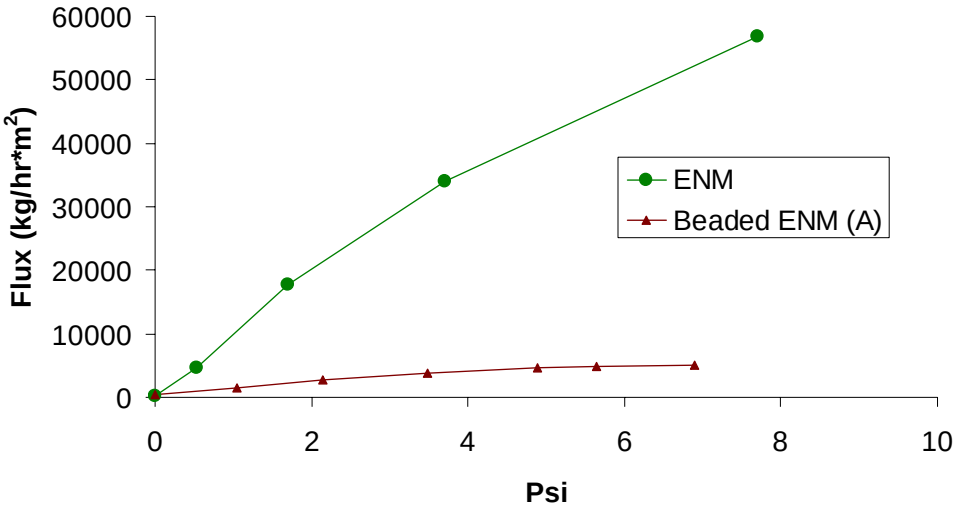

Figure 5.8: Water flux permeation of as-spun ENM and Beaded ENM (A)

5.3.2 Comparison of water flux performance of grafted and as-spun ENMs

The contact angle study has shown that after grafting a hydrophilic layer on the surface of ENM the surface is easily wetted and hence it is anticipated that the flux performance of the grafted membrane should improve. However according to the flux profile shown in Figure 5.9, the non-grafted ENM had a much better flux performance than the grafted ENM. This can be explained in terms of pore size. According to the pore size distribution Figures, non grafted ENM had the largest pores and the bubble point is four times more than the grafted ENM. Hence a smaller pressure is required to achieve the same flux. In this situation the determinant factor for the flux performance is pore size rather than the surface chemistry.

5.3.3 Comparison of water flux performance of grafted ENM and commercial membranes

The flux performance of grafted ENM and commercial membrane is also reflected in Figure 5.9. When the pore sizes are kept the same and the surface hydrophilicity is varied, the flux performance can be enhanced. This is evident in the case of HVHP and HVLP. Despite having a similar pore size (~ 0.45 µm), HVLP had a higher flux than HVHP attributed to hydrophilic surface layer. Interestingly, although the pore size distribution of grafted ENM and HVLP was very similar and both of them had LEPw of zero, their flux profile is different. Grafted ENM had a higher water flux than HVLP. This can be explained by the difference in the membrane porosity of the membranes. ENMs have a much higher porosity and this leads to a higher flux as compared to HVLP membranes which have lower porosity. Hence having an asymmetric MF electrospun membrane through surface modification is advantageous.

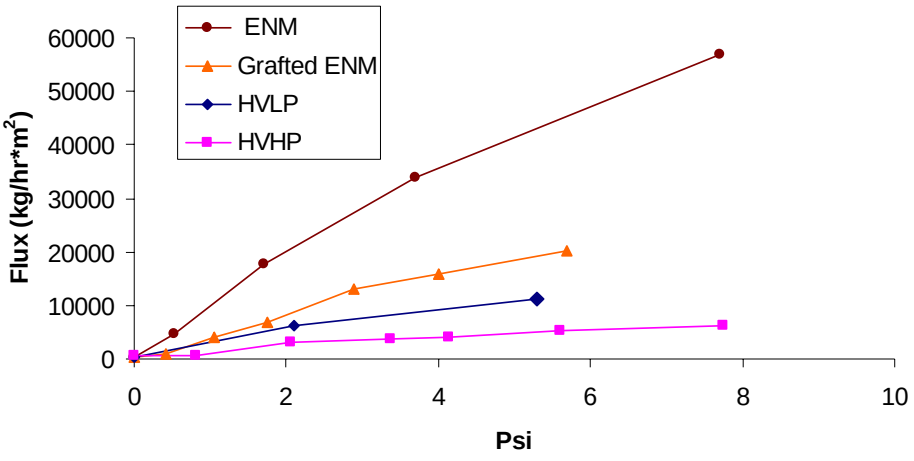

Figure 5.9: Water flux permeation of ENM, grafted ENM, HVLP and HVHP

5.4 Separation Study

To assess the developed ENM's ability to function as MF membranes, a simple model using polystyrene micro-particles (sigma-aldrich, USA) was employed [Gopal (2006)]. The spinning conditions for the non-grafted ENM used for separation study was 15 percent wt./vol PVDF prepared in DMAC/AC mixture (1:1 v/v). This membrane has a bubble point of 3.2 μm using the capillary flow porometer.

PS microparticles of 1,5,10 μm were used to determine the separation performance of the non-modified ENMs. A solution of 500 ppm was prepared for each particle size and a calibration curve of concentration against absorbance was obtained for each particle diameter using a UV/Vis Spectrophotometry. The membranes were wetted with 50% ethanol and then placed in the dead end filtration set up. Pressure of the cell was gradually increased to ensure that the membrane was completely wetted and then water in the cell was replaced. The flux of the pure water was determined first followed by the separation of 100 ml of PS micro-particles solutions. The separation flux was measured for every 5 ml of permeate collected. Presence of any PS micro-particles was detected via the UV/Vis Spectrophotometer and the concentration was determined using the calibration curve. The separation experiment was stopped after 50 ml of permeate was collected. The remaining PS solution was removed and the cell rinsed thrice, without removing the ENM. The cell was refilled with distilled water and the water flux was determined again. The separation factor (SF) was determined using the formula below:

$$SF = (1 - \frac{C_{permeate}}{C_{feed}}) \times 100\%$$

Where $C_{permeate}$ and C_{feed} are the PS concentration in the permeate and in the feed.

According to the pore size distribution results, it is anticipated that the non-grafted ENM should be able to separate the 10 and 5 μm micro-particles effectively. The separation factor for the 10 μm particle solution was 96%. This corresponds well with pore size measured for the ENM as stated in Table 5.3. The flux was also recovered completely, indicating no permanent fouling of the ENM. From Figure 5.10b it could be observed that at the end of experimental run, there were no micro-particles trapped on the membrane surface. The stirring in the membrane module was sufficient enough to lift the PS particles from the surface of the membrane. Thus the flux was unaffected. In the case of the 5 μm particles, the separation was 91%, lower compared to 10 μm particles.

Presence of more pores larger than 5 μm in the ENM allows some 5μm particles to permeate through compared to 10 μm particles. Upon rinsing, there was no significant drop in water flux. However, Figure 5.10c showed some particle deposition on the surface. Nevertheless, the stirring was still sufficient to prevent severe deposition of PS beads on the surface of the membrane. The separation of 1 μm particles was more peculiar at first glance. The flux reduction was instantaneous at the onset of the experiment. To alleviate this problem, the concentration of the feed

solution was reduced to 100 ppm to decrease the amount of micro-particles present. Even after lowering the concentration, the flux was greatly reduced and not recovered. The separation was the highest at 98%. This separation does not correlate with any of the membrane characterization data obtained previously. Figure 5.10d revealed a layer of particle deposition on the surface of the ENM. As the micro-particles are small, they were able to pack closely together, reducing the effective pore size of the ENM significantly at the surface. This dense 'cake' acted as the separating layer for the ENM. This accounts for the unusually high separation factor. It should be noted that the velocity of particle migration away form the membrane surface due to the superimposition of Brownian diffusion, lateral migration and shear induced diffusion exhibits a minimum when the particle size is between 0.1 and 1 μm [Alvarez (1999)]. The separation of 1 μm particles with the ENM falls into this category. This explains the severe particle deposition observed for the 1 μm separation. This caused the ENM to be irreversibly fouled and the initial flux could not be recovered. Furthermore, for the same feed concentration, a smaller particle will have a greater number density than larger particles. Thus there are more 1 μm particles in a 500 ppm solution as compared to a 5 μm solution and even greater than a 10 μm solution. This increases the probability of fouling.

Particle size (μm)	Pressure (psi)	Feed (ppm)	Water flux start of expt (kg/m^2h)	Feed flux (kg/h)	Water flux end of expt (kg/h)	Separation factor (%)
10	8.3	500	133	133	133	96
5	8.3	500	200	200-133	200	91
1	8.3	500	467	Instantaneous drop in flux		
1	9.5	100	1300	1066-530	530	98

Table 5.3: Separation of 1, 5, and 10 μm PS micro-particles using ENM

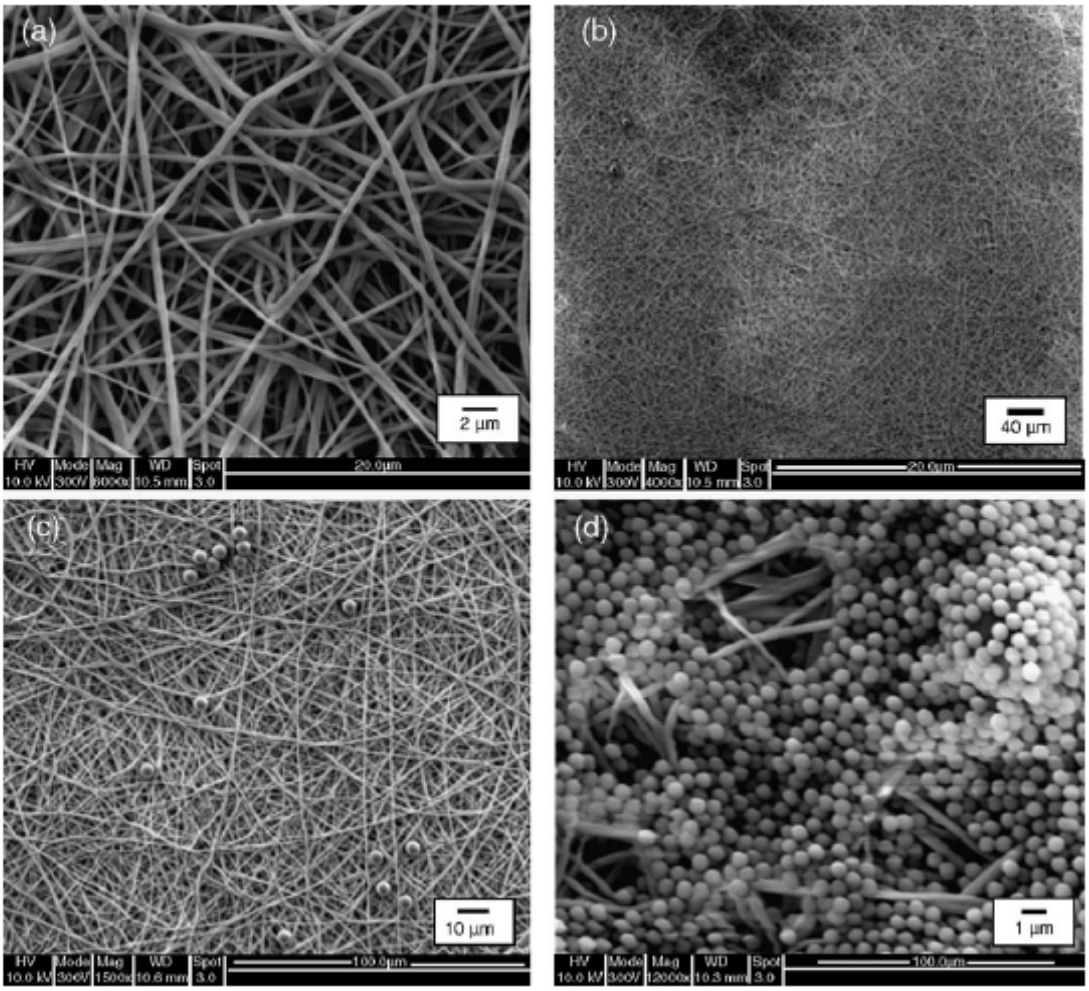

Figure 5.10: FESEM micrographs of PVDF membrane: (a) before separation, (b) after 10 μm (c) after 5 μm, and (d) after 1 μm separation.

5.5 Conclusion

There is a potential for as-spun microfiltration ENMs to remove micro-particles in the range of 5 to 10 μm effectively without any damage to the membrane. This separation characteristic correlates with the largest pore detected which is 3.2 μm. Hence particles above the bubble point of the ENM will be rejected efficiently. Thus the capillary flow porometer is capable in giving a good gauge of the separation rejection of a membrane.

The surface of ENM has been successfully grafted with PMAA by plasma induced graft co-polymerization. The grafted ENM showed a higher grafting density than HVHP, primarily due to its higher surface area for grafting. Through grafting, the pore size of the ENM was significantly reduced from 3.56 to 0.88 μm and hence it is anticipated that this surface grafted ENM would reject particles above 1 μm. After grafting, the as-spun ENM was transformed into a microfiltration membrane, similar in pore-size distribution to a commercial (0.45 μm) membrane but has a significantly larger flux performance as shown in Figure 5.9. This indicated that through grafting, it is possible to develop high flux electrospun nanofiber membranes with reduced pore size.

The microfiltration ENMs can be employed as pre-filters to remove particulate contaminants from waste-water and hence serve to take off the load from the final filter such as UF, NR or RO filters. The best prefilters have a high internal surface

area and it has been established that fibrous depth filters provide enormous particle loading capacity compared with membrane filters.

Recommendations for Further Work

Through this work, it has been shown that ENMs can act as prefilters and through surface modification, a ‘tighter’ microfiltration membrane can be achieved. It was also shown that ENMs possess a high flux rate and this is of great advantage in a commercial and economical context. This work can be extended by developing a high flux, low pressure drop UF and NF membrane via surface modification. The separation and fouling tendency of these developed membranes should be studied and it would worthwhile to make comparisons with commercial membranes.

References

Alvarez JR

Pressure driven membrane processes, in: Membrane applications in the food and dairy industry

Coca J, S. Luque S (Eds.), University of Oviedo, Spain, 1999, p. 23

Bergshoef MM and Vancso GJ

Transparent Nanocomposites with ultrathin electrospun nylon-4,6 fiber reinforcement

Adv. Mater., 1999, 11, p. 1362

Bognitzki M, Hou H, Ishaque M, Frese T, Hellwig M, Schwarte C, Schaper A, Wendorff JH and Greiner A

Polymer, metal, and hybrid nano- and mesotubes by coating degradable polymer template fibers (TUFT Process)

Adv. Mater., 2000, 12, p. 637

Bryjak M, Gancarz I, Pozniak G and Tylus W

Modification of polysulfone membranes 4. Ammonia plasma treatment

Eur. Polym.J., 2001, 38, p.717

Caruso RA, Schattka JH and Greiner A

Titanium dioxide tubes from sol-gel coating of electrospun polymer fibers

Adv. Mater.,2001, 20, p.1577

Casper CL, Stephens JS, Tassi NG, Chase DB and Rabolt JF

Controlling surface morphology of electrospun polystyrene fibers:

Effect of humidity and molecular weight in the electrospinning process
Macromolecules, 2004, 37, p. 573

Cen L, Neoh KG and Kang ET
Surface Functionalization Technique for Conferring Antibacterial Properties to Polymeric and Cellulosic Surfaces
Langmuir, 2003, 19, p.10295

Chan CM, Ko TM and Hiraoka H
Polymer surface modification by plasmas and photons
Surface Science Reports, 1996, 24, p. 1

Chatelier RC, Xie X, Gengenbach TR and Griesser HJ
Quantitative Analysis of Polymer Surface Restructuring
Langmuir, 1995, 11, p. 2576

Christanti Y and Walker LM
Surface tension driven jet break up of strain-hardening polymer solutions
J. Non-newton. Fluid, 2001, 11, p.9

Chua KN, Lim WS, Zhang P, Lu H, Wen J, Seeram R, Leong KW, Mao HQ
Stable immobilization of rat hepatocyte spheroids on galactosylated nanofiber scaffold
Biomaterials, 2005, 26, p. 2537

Choi JS, Lee SW, Jeong L, Bae SH, Min BC, Youk JH and Park WH
Effect of organosoluble salts on the nanofibrous structure of electrospun poly(3-hydroxybutyrate-co-3-hydroxyvalerate)

Int.J.Bio.Macromolecules, 2004, 4, p. 249

Choi SW, Jo SM, Lee WS and Kim YR

An electrospun poly(vinylidene fluoride) nanofibrous membrane and its battery applications

Adv. Mater., 2003, 15, p. 2027

Clouet F and Shi MK

Interactions of polymer model surfaces with cold plasmas: Hexatriacontane as a model molecule of high-density polyethylene and octadecyl octadecanoate as a model of polyester. I. Degradation rate versus time and power

J. Appl. Polym. Sci, 1992, 46, p.1955

Cooley JF

Apparatus for electrically dispersing fluids

1902, U.S. Patent no.: 692631

Dohany JE and Robb LE

Kirk-Othmer encyclopaedia of chemical technology

Vol. 11, 3rd Edn., Wiley Interscience, New York, 1980, edited by Othmer DF

Fane, AG and Fell CJD

A review of fouling and fouling control in ultrafiltration

Desalination, 1987,62, p.117

Feng L, Li SH, Li HJ, Zhai J, Song YL, Jiang L and Zhu DB

Super hydrophobic surface of aligned polyacrylonitrile nanofibers

Angew. Chem.Int. Ed., 2002,41, p. 1221

Fong H, Chun J, Reneker DH

Beaded nanofibers formed during electrospinning

Polymer, 1999, 40, p.4585

Fong H, and Reneker DH

Elastomeric nanofibers of styrene-butadiene-styrene triblock copolymer

J. Polym. Sci. Pt.B-Polym.Phys., 1999, 37, p.3488

Formhals A

Process and apparatus for preparing artificial threads.

US Patent. 1934, 1,975,504

France RM and Short RD

Plasma Treatment of Polymers: The Effects of Energy Transfer from an Argon Plasma on the Surface Chemistry of Polystyrene, and Polypropylene. A High-Energy Resolution X-ray Photoelectron Spectroscopy Study

Langmuir, 1998, 14, p. 4827

Glennon D, Smith J R, Nevell RT, Begg D, Mason SE, Watson KL, Tsibouklis J

An atomic force microscopy study of the effect of tensile loading and elevated temperature on polyvinylidene fluoride from flexible oil pipelines

J. Mat. Sci., 1997, 32, p 6227

Gibson P, Gibson HS and Rivin D

Transport properties of porous membranes based on electrospun nanofibers
Colloids Surf. A: Physicochem. Eng. Aspects, 2001, 187/188, p. 469

Gopal R, Kaur S, Ma Z, Ramakrishna S, Matsuura T
Electrospun nanofibrous filtration membrane
J. Mem. Sci., 2006, 281, p.581

Gouma PI
Nanostructured polymorphic oxides for advanced chemosensors
Rev. Adv. Mater.Sci., 2003, 5, p. 147

Graham K, Ouyang M, Raether T, Grafe T, McDonald B, Knauf P
Polymeric nanofibers in air filtration applications fifteenth annual technical
Conference & Expo of the American Filtration & Separations Society, Galveston, TX: 9-12 April 2002

Greet V, Iksoo C, Rosenblatt J, Peeters J, Dijck AV, Mensch J, Noppe M and Brewster ME
Incorporation of drugs in an amporphous state into electrospun naofibers composed of a water insoluble, non-biodegradable polymer
J.Control Release, 2003, 92, p. 349

Hong C, Hsieh YL
Enzyme immobilization on ultrafine cellulose fibers via poly(acrylic acid) electrolyte grafts
Biotec. & Bioeng., 2005, 90, p.405

Hsu CM, Shivakumar S

N,N-Dimethylformamide additions to the solution for the electrospinning of poly(e-caprolactone) nanofibers

Macromol. Mater. Eng., 2004, 289, p. 334

Huang ZM, Zhang YZ, Kotaki M, Ramakrishna

A review on polymer nanofibers by electrospinning and their applications in nanocomposites

Compos. Sci Technol., 2003, 63, p.2223

Huang C, Chen S, Lai C, Reneker DH, Qiu H, Ye Y, Hou H

Electrospun polymer nanofibers with small diameters

Nanotechnology, 2006, 17, p. 1558

Iwata H, Oodate M, Uyama Y, Amemiya H, Ikada Y

Preparation of temperature-sensitive membranes by graft polymerization onto a porous membrane

J. Mem. Sci., 1991, 55, p.119

Jarusuwannapoom T, Hongrojjanawiwat W, Jitjaicham S, Wannatong L, Nithitanakul M, Pattamaprom C, Koombhongse P, Rangkupan R and Supaphol P.

Effects of solvents on electro-spinnability of polystyrene solutions and morphological appearance of resulting electrospun polystyrene fibers

Euro. Polym.J., 2005, 41, p.873

Kato K, Uchida E, Kang ET, Uyama Y, Ikada Y

Polymer surface with graft chains

Prog. Polym. Sci., 2003, 28, p.209

Kaur S, Kotaki M, Ma Z, Gopal R, Ramakrishna S and Ng SC

Oligosaccharide functionalized nanofibrous membrane

Int. J. Nanoscience, 2006, 5,p. 1

Keith S

Handbook of industrial membranes

Oxford : Elsevier Advanced Technology, 1995

Klein E

Affinity membranes: Their Chemistry and Performance in Adsorptive Separation Processes,

John Wiley and Sons, 1991

Koombhongse S, Liu W and Reneker DH

Flat polymer ribbons and other shapes by electrospinning

J. Polym. Sci. Polym. Phys., 2001, 39,p. 2598

Kou RQ, Xu Z.K, Deng HT, Liu ZM, Seta P, Xu Y

Surface Modification of Microporous Polypropylene Membranes by Plasma-Induced Graft Polymerization of α-Allyl Glucoside

Langmuir, 2003, 19, p.6869

Kroschwitz JI

Concise Encyclopedia of Polymer Science and Engineering

New York: Wiley, 1990

Liu GJ, Qiao LJ and Guo A

Diblock copolymer nanofibers

Macromol., 1996, 29, p. 5508

Liu HQ and Hsieh YL

Ultrafine fibrous cellulose membranes from electrospinning of cellulose acetate

J. Polym. Sci. Pol. Phys. 2002,40, p.2119

Loeb S and Sourirajan S

Saline water conversion - II : Based on symposia sponsored by the Division of Water and Waste Chemistry at the 139th and 141st Meetings of the American Chemical Society, March 27, 1961 and March 27-8, 1962

Adv. Chem. Ser., 1962,38, p.117

Luu YK, Kim K, Hsiao BS, Chu B, Hadjiargyrou M

Development of a nanostructured DNA delivery scaffold via electrospinning of PLGA and PLA-PEG block copolymers

J. Control Release, 2003, 89, p. 341

Ma M, Hill RM, Lowery JL, Fridrikh SV and Rutledge GC

Electrospun poly(styrene-block-dimethylsiloxane) block copolymer fibers exhibiting superhydrophobicity

Langmuir, 2005, 21, p. 5549

Ma PX and Zhang R

Synthetic nano-scale fibrous extracellular matrix

J.Biomed. Mater. Res., 1999, 46, p. 60-72

Ma Z, Kotaki,M, Ramakrishna S

Surface modified nonwoven polysulphone (PSU) fiber mesh by electrospinning: A novel affinity membrane

J. Mem.Sci., 2006 (a), 272, 179-187

Ma Z, Kotaki,M, Ramakrishna S

Immobilization of Cibaron blue F3GA on electrospun polysulphone ultra-fine fiber surfaces towards developing an affinity membrane for albumin adsorption

J. Mem.Sci., 2006 (b), 272, 179-187

Mark CP

Handbook of Industrial Membrane Technology

Noyes Publications, New Jersey, U.S.A, edited by Mark CP, 1990

Matsuura T

Synthetic Membranes and Membrane Separation Processes

Publishers, Boca Raton, CRC Press, 1994

Mit-uppatham C, Nithitanakul M and Supaphol P

Ultrafine Electrospun polyamide-6 fibers: Effect of solution conditions on morphology and average fiber diameter

Macromol. Chem. Physic., 2004, 205,p. 2327

Miwa M, Nakajima A, Fujishima A, Hashimoto K and Watanabe T

Effects of the surface roughness on sliding angles of water droplets on superhydrophobic surfaces

Langmuir, 2000, 16, p. 5754

Morozov VN, Morozova TY, and Kallenbach NR

Atomic force microscopy of structures produced by electrospraying polymer solutions

Int. J. Mass.Spectron., 1998, 178, p.143

Mulder M

Basic Principles of Membrane Technology

Kluwer Academic, 1996

Nakagawa K and Ishida Y

Annealing effect in poly(vinylidene fluoride) as revealed by specific volume measurements, differential scanning calorimetry and electron microscopy

J. Polym. Sci. Phys., 1973, 11, p. 2153

Nunes SP and Peinemann KV

Membrane Technology in the Chemical Industry

Wiley-VCH verlag GmbH, Weinheim, Germany, 2001

Ondarcuhu T and Joachim C

Drawing a single nanofiber over hundreds of microns

Europhys. Lett., 1998, 42, p. 215

Osada Y, Honda K and Ohta M

Control of water permeability by mechanochemical contraction of poly(methacrylic acid)-grafted membranes

J. Mem.Sci., 1986,27, p.327

Penn LS and Wang H

Chemical modification of polymer surfaces: A review

Polym. Adv. Techno.,1994, 5, 809-817

Ramaseshan R, Sundarrajan S, Liu Y, Barhate RS, Lala NL and

Ramakrishna S

Functionalized polymer nanofibre membranes for protection from chemical warfare stimulants
Nanotechnology, 2006, 17, p. 2947

Seeram R, Fujihara K, Teo WE, Lim TC, Ma Z

An introduction to electrospinning and nanofibers

World scientific publishing, Singapore, 2005

Shin M, Ishii O, Sued T, Vacanti JP

Contractile cardiac grafts using a novel nanofibrous mesh

Biomaterials, 2004, 25, p.3717

Shummer P, Tebel, KH

A new elongational Rheometer for polymer solutions

J.Non-newton fluid, 1983, 12, 331-347

Son WK, Youk JH, Lee TS and Park WH

Electrospinning of ultrafine cellulose acetate fibers: studies of a new solvent system and deacetylation of ultrafine cellulose acetate fibers

J.Polym. Sci. Pt. B-Polym. Phys., 2004, 42, p.5

Strathmann H

Membrane separation processes

J.Mem.Sci., 1981, 9, p. 121

Suthar A and Chase G

Nanofibers in filter media

Chemical Engineer, 2001, 726, p. 26

Suzuki M, Kishida A, Iwata H, Ikada Y

Graft copolymerization of acrylamide onto a polyethylene surface pretreated with glow discharge

Macromolecules, 1986, 19, p.1804

Taylor GI

Electrically driven jets

Proc. R. Soc. London, Ser. A 1969; 313, p.453

Timothy H G and Kristine M G

Nanofiber webs from electrospinning

Proceedings of the Fifth International Conference, Stuttgart, Germany, March 2003

Toyomoto K and Higuchi A

Membrane Science and Technology

New York : M. Dekker, edited by Osada Y and Nakagawa T, 1992

Tsai PP, Schreuder-Gibson H, Gibson P

Different electrostatic methods for making electret filters

J Electrostatics, 2002, 54,p.333

Uchida E, Uyama Y, Ikada Y

Sorption of low-molecular-weight anions into thin polycation layers grafted onto a film

Langmuir, 1993, 9, p.1121

Wang P, Tan KL, Kang ET and Neoh KG

Plasma-induced immobilization of poly(ethylene glycol) onto poly(vinylidene fluoride) microporous membrane

J. Mem. Sci., 2002, 195, p. 103

Wang X, Drew C, Lee SH, Senecal KJ, Kumar J, Samuelson LA
Electrospun nanofibrous membranes for highly sensitive optical sensors
Nano.Lett., 2002, 11, p.1273

Wang X, Fang D, Yoon K, Hsiao BS, Chu B
High performance ultrafiltration composite membranes based on poly(vinyl alcohol) hydrogel coating on crosslinked nanofibrous poly(vinyl alcohol) scaffold
J. Mem. Sci., 2006, 278, p.261

Wannatong L, Sirivat A and Supaphol P
Effects of solvents on electrospun polymeric fibers: preliminary study on polystyrene
Polym., Int., 2004, 53, p.1851

Wavhal DS and Fisher ER
Hydrophilic modification of polyethersulfone membranes by low temperature plasma-induced graft polymerization
J.Mem. Sci., 2002,209, p.255

Wavhal DS and Fisher ER
Membrane surface modification by plasma induced polymerization of acrylamide for improved surface properties and reduced protein fouling
Langmuir 2003, 19, p. 79-85

William JM
Method of dispersing fluids
1902, U.S. Patent no.: 705691

Zeng J, Xu X, Chen X, Liang Q, Bian X, Yang L, Jing X

Biodegradable electrospun fibers for drug delivery

J. Control. Release, 2003, 92, p. 227

Zuwei M, Wei H, Thomas Y, Seeram R

Grafting of Gelatin on electrospun poly9caprolactone) nanofibers to improve endothelial cell spreading and proliferation and to control cell orientation

Tissue Eng., 2005, 11, p.1149